

Integrated optical devices for lab-on-a-chip biosensing applications

M.-Carmen Estevez, Mar Alvarez and Laura M. Lechuga*

Nanobiosensors and Bioanalytical Applications Group, Research Center on Nanoscience and Nanotechnology (CSIC) & CIBER-BBN. Campus UAB, 08193 Bellaterra, Barcelona, Spain

*Email: Laura.lechuga@cin2.es

Phone: +34-935868012

Fax: +34-935868020

Abstract. The application of portable, easy-to-use and highly sensitive lab-on-a-chip biosensing devices for real-time diagnosis could offer significant advantages over current analytical methods. Integrated optics-based biosensors have become the most suitable technology for lab-on-chip integration due to their ability for miniaturization, their extreme sensitivity, robustness, reliability, and their potential for multiplexing and mass production at low cost. This review provides an extended overview of the state-of-the-art in integrated photonic biosensors technology including interferometers, grating couplers, microring resonators, photonic crystals and other novel nanophotonic transducers. Particular emphasis has been placed on describing their real biosensing applications and wherever possible a comparison of the sensing performances between each type of device is included. The way towards achieving operative lab-on-a-chip platform incorporating the photonic biosensors is also reviewed. Concluding remarks regarding the future prospects and potential impact of this technology are also provided.

Short title: M.C. Estevez, M. Alvarez and L.M. Lechuga: Integrated optical biosensors.

PACS: 87.85.fk, 42.82.Et, 07.07.Df, 07.07.Mp, 07.60.Ly, 87.85.Rs

Keywords: Photonic biosensors, evanescent wave detection, lab-on-a-chip, biofunctionalization, silicon photonics.

1. Introduction

Biosensors are devices able to detect a specific substance by converting the recognition from a biological entity (i.e. DNA, antibody, enzyme,...) into an electrical signal that can be further processed and related to the concentration of the substance under analysis. Biosensors can provide selective, sensitive, fast, direct and cost-effective analyses. In addition, they can perform tests in real-time without using fluorescent labels or amplification steps and with a minimum volume of samples and reagents [1]. As compared to standard techniques which are usually time-consuming, expensive and require labelling and trained personal, biosensing technology offers clear advantages.

Lab-on-a-chip (LOC) are miniaturized devices in which all functionalities are integrated in the same platform, from sample preparation to signal delivery [2]. Ideally a LOC device should contain enough hard wired intelligence and robustness to be used by non-skilled personal and should deliver the results directly to a central monitoring station. It is clear that achieving a small, portable and easy-to-use lab-on-a-chip device for diagnostics could offer significant advantages over standard methods. Although significant progress has been accomplished at the LOC field during last years, very few stand-alone devices have emerged [3]. Most of current devices are simple planar microfluidic devices which do not incorporate the detection and after the reaction has taken place, the read-out must be done with complex instrumentation in laboratory settings. That is the main reason why incorporating “on-chip” detection by using biosensors is a new technology that shows great promise. Main application fields of this technology can be clinical diagnostics, environmental monitoring, chemical and biological warfare surveillance, food industry and veterinary and industrial process control, among others. By using this advanced technology, diagnosis in developing countries could become an important achievement for the near future.

Photonic biosensors are well-established technologies for the sensitive monitoring of molecular interactions. They could afford the requirements for the “on-chip” detection in lab-on-a-chip platforms due to their outstanding characteristics of sensitivity, label-free and real-time detection. The detection principle of most optical biosensors is based on the evanescent field detection. In the evanescent wave mechanism (see Figure 1), a bioreceptor layer is immobilized onto the surface of a waveguide; the exposure to the partner analyte produces a biomolecular interaction affecting the guiding properties of the waveguide (concretely, a variation of the refractive index) via the modification through the evanescent field. The variation of the refractive index can be evaluated by any of the waveguiding optical properties (intensity, phase,

1
2
3 resonant momentum, polarization,...) and this variation can be correlated with the concentration
4 of the analyte and with the affinity constant of the interaction, resulting in a quantitative value
5 of the interaction.
6
7

8
9
10 As the evanescent wave decays exponentially while it penetrates into the outer medium, it only
11 detects changes taking place on the surface of the waveguide, since the intensity of the
12 evanescent field is much higher in this particular region. For most waveguide systems, this
13 decay length is on the order of 0.1-1 μm . For that reason, it is not necessary to carry out a prior
14 separation of non-specific components (as in conventional analyses) because any change in the
15 bulk solution will hardly affect the sensor response. Therefore, the most significant advantages
16 of evanescent-based mechanism are the highly sensitive and specific label-free detection of
17 target molecules or biochemical reactions in real time, with reduced nonspecific binding, which
18 makes this detection mechanism one of the most useful for detection of targets in complex real
19 samples.
20
21
22
23
24
25

26
27
28 The most common optical evanescent wave biosensor is the Surface Plasmon Resonance (SPR)
29 device [4] based on the variation of the reflectivity on a metallic layer in close contact with a
30 dielectric media. The SPR biosensor has been widely developed and commercialized and
31 hundreds of publications have demonstrated its outstanding performance to evaluate complex
32 biosensing interactions [4]. But SPR sensor has a relatively large size and its miniaturization in
33 lab-on-chip platforms is complex. Moreover, the sensitivity is usually limited to the nanomolar
34 range, which is extremely useful in diverse applications [5-7] but not enough for applications
35 requiring lower detection levels (pM-fM or even single-molecule), which are usual in the
36 clinical practice.
37
38
39
40
41
42

43
44 Photonic sensors based on integrated optics (IO) could solve the aforementioned SPR problems,
45 as they can be easily miniaturized and they offer high potential for chip integration; moreover,
46 by using evanescent wave as detection mechanism, sensitivities can be extremely high (pM in a
47 label-free scheme). Moreover, integrated optics allows a great flexibility in the materials and
48 structures selection and fabrication of arrays of sensors with the same characteristics within the
49 same chip for multiplexing analysis can be afforded. Materials employed in IO devices are Si,
50 Si_3N_4 , SiON, SiO_2 or polymers, and techniques such as ion-diffusion in glass, chemical vapour
51 deposition, spin-coating, nanoimprinting, electron beam lithography, etc are commonly
52 employed for the fabrication. By using silicon photonics technology, additional advantages such
53 as robustness, reliability, low power consumption and potential for mass production with
54 consequent reduction of production costs are added. Other technologies as III-V or lithium
55
56
57
58
59
60

1
2
3 niobate, often used in optical telecommunications, have shown less suitability for IO biosensors
4 as they are more complex and expensive.
5
6

7
8 Most of the refractive index IO sensors rely on the induced changes of the effective refractive
9 index by the biomolecular interaction in the evanescent area. In order to achieve highest
10 sensitivity, the waveguiding structure must be optimized looking for a maximum change of the
11 effective refractive index due to the sensing bilayer. Sensitivity is a complex parameter
12 involving geometry, material and working wavelength of the waveguide, and also other aspects
13 such as the chemical activation of the surface, the biofunctionalization method and the
14 resolution and noise of the optical read-out system. In addition, fluidics must be taken into
15 account (i.e. flow cell volume, way of sample injection, diffusion, dispersion). Each of these
16 aspects must be properly designed and optimized before delivering a functional biosensor
17 device. Integrated optical sensors such as grating-couplers, interferometers, photonic crystal,
18 microring resonators, slot waveguides or silicon wires have been extensively studied in the last
19 years [8-12], but so far only few of them are commercially available.
20
21
22
23
24
25
26
27
28

29 One of the main advantages of the IO technology is the possibility to integrate all the functions
30 (chemical, optical, microfluidics and electronics) in one single platform offering an ideal
31 solution for the implementation of truly lab-on-a-chip devices. This area is still in its infancy,
32 but remarkable progress has been achieved during last years [3,13]. This is reflected in the
33 increasing amount of publications addressing new or optimized sensing configurations.
34
35
36
37
38

39 In this chapter, an overview of the main integrated optical sensors will be presented with special
40 focus on the most relevant ones in terms of sensing performance and integration capability, and
41 whose feasibility for label-free biosensing has been proven. For each of them, a brief description
42 of its operating principle, design, fabrication and read-out resolution will be presented, and,
43 when reported, the biosensing dynamic range and detection limit will be summarized.
44 Application in clinical diagnostics, environmental monitoring, or in food and agroalimentary
45 industry will be included as well as a brief section describing the commercial devices already on
46 the market. One of the crucial aspects that will be discussed is the way towards a truly lab-on-a-
47 chip integration, although few examples of completely integrated platforms can be found in the
48 literature. Finally, an outlook of the future prospects of this technology will be discussed.
49
50
51
52
53
54
55
56

57 **2. Biofunctionalization and immobilization strategies**

58 The selection of an appropriate procedure to immobilize the biological element on the sensor
59 surface has become a critical step in the biosensor area, and enormous efforts are continuously
60 invested in order to optimize novel strategies according with the application. The

1
2
3 immobilization process should not only guarantee an efficient coverage of the transducer
4 surface with the biomolecules, while keeping intact their properties (functionality, structure,
5 biological activity, affinity, specificity...), but it should also ensure their stability for storage
6 and regeneration. Moreover, most of the applications, such as clinical and medical diagnosis,
7 agroalimentary analysis, or environmental field surveillance, require well-defined surfaces with
8 biocompatible properties, minimizing non-specific adsorption when analyzing complex real
9 samples. The choice of the most effective strategy of immobilization which combines the above
10 considerations usually becomes the key factor which turns a sensing device into a valid and
11 applicable analytical tool with the required quality standards. Moreover, the bioreceptor layer
12 directly affects the reproducibility, selectivity and resolution of any sensor device.
13
14
15
16
17
18
19

20
21 A wide variety of biomolecules can be used as bioreceptors, i.e. antibodies, nucleic acid
22 sequences, peptides, enzymes, cell receptors and many others. The selected biomolecule is
23 dictated by the application and must be chosen to be highly specific for the target molecule and
24 stable enough to be immobilized without losing functionality. Several types of routes can be
25 used to biofunctionalize the sensor surface: (i) physical adsorption by direct deposition of the
26 biomolecule; (ii) covalent binding of the biomolecule to the surface (using a cross-linker
27 previously immobilized on the surface or following more complex strategies [14]); (iii) non-
28 covalent interactions to a previously deposited active layer, either by non-specific electrostatic
29 interactions or by non-covalent affinity binding (i.e. biotin-avidin systems, His-Tag system,
30 Protein A/G for antibodies) (iv) physical entrapment in a polymer layer. Figure 2 summarizes
31 the general immobilization strategies.
32
33
34
35
36
37
38
39

40
41 Physical adsorption is a simple strategy based on hydrophobic and electrostatic interactions
42 between the biomolecule and the surface, but it can lead to the easy desorption of the active
43 receptors under flow conditions and also when regeneration cocktails are applied to break the
44 interaction event (which usually implies high or low pH solutions, salt concentrations, organic
45 solvents, etc.). Moreover, issues related to reproducibility together with undesired folding of the
46 biomolecules onto the surface are common drawbacks of this strategy which makes it not
47 advisable in most of the cases even despite its simplicity.
48
49
50
51
52

53
54 Covalent binding can be made through one of the chemical groups of the biomolecule. It is
55 recommended to use a group whose blocking does not compromise the overall functionality of
56 the biomolecule. Amino, carboxylic or thiol groups are the preferred option to couple proteins.
57 For nucleic acids immobilization, it is possible to take advantage of the versatility of the DNA
58 synthesis which allows the incorporation of reactive groups at the end of the sequence. Specially
59 difficult is the attachment of antibodies in an oriented way (leaving the affinity binding sites
60

1
2
3 free), which can be done by controlled binding through the carbohydrates groups of the constant
4 region or by using affinity proteins (such as A or G Protein) [15]. Another non-covalent affinity
5 binding strategy is based on the biotin-avidin system, through the formation of a sandwich-like
6 layer (biotin on the surface/avidin/biotinylated biomolecule) [14-16].
7
8
9

10
11 Before the biofunctionalization step, a previous chemical activation of the sensor surface is
12 always needed. Silicon, silicon oxide and silicon nitride are conventional materials commonly
13 used for integrated optical transducers which can be functionalized using the well-known silane
14 chemistry. Silicon-based surfaces require a prior activation step to oxidize the surface and to
15 expose the silanol groups for crosslinking with the silane. Whereas silicon oxide is hydrophilic,
16 silicon nitride is an electronically neutral non-porous material, whose modification is usually
17 not straightforward. In the case of silicon nitride, methods are based on an initial etching to
18 remove the native SiO₂ layer to further be oxidized to form a new oxide layer [17]. Other
19 strategies involve the derivatization of the Si-H and Si-N groups of the silicon nitride using
20 more drastic conditions [18-21]. The activated surface is subsequently modified with
21 organosilanes forming a silane layer with exposed reactive groups susceptible to react with the
22 bioreceptor. Hundreds of different organosilanes with a wide variety of structures, length,
23 functionality and chemical and physical properties are nowadays commercially available,
24 although the most commonly employed are those with short alkyl chain (i.e. propyl, butyl),
25 ending in amino, thiol, epoxy or carboxylic groups.
26
27
28
29
30
31
32
33
34
35
36

37 As a first step, evaluation of the biosensor capability is done using purified or spiked samples in
38 buffer. But in order to assess the real performance of any device, complex samples which
39 contain high concentration of non-specific molecules, such as blood, urine, serum, saliva, tears,
40 cerebrospinal or medullar fluids should be tested. For preparation of the receptor layer which
41 must avoid matrix effects and large background signals, less conventional reagents that provide
42 a more hydrophilic and biocompatible and antifouling surface are increasingly being used such
43 as dextran polymer [22] or poly(ethylene) glycol (PEG) derivatives [23-28].
44
45
46
47
48
49

50 Overall, to achieve the full potential of the optical sensing devices, the choice of the surface
51 modification, the biofunctionalization procedures, and the type and conditions of the assay
52 become as relevant and crucial as the development and optimization itself of the integrated
53 optics-based sensing structures.
54
55
56
57

58 **3. Biosensors based on Integrated Optics**

59
60

1
2
3 In this Section, an overview of the main biosensing technologies based on integrated optics will
4 be presented. The main driving force behind the development of integrated optical biosensors is
5 to push the sensitivity for label-free detection of minimum amounts of substances, which are the
6 concentration normally found in human fluids at the starting of a disease (as cancer) or in
7 contaminated water or food or in a biowarfare attack: the lower the limit of detection, the earlier
8 the disease or the pollutant could be detected. Limit of detection (LOD) and sensitivity are the
9 most important parameters which define the sensor performance. The sensitivity is mostly
10 referred to the strength of light-matter interaction. Limit of detection can be defined as the
11 smallest amount of analyte that produces a quantifiable output signal and will depend on the
12 resolution of the optical read-out system and therefore it is strongly related to the experimental
13 noise. Contributions from laser or light source intensity fluctuations, microfluidics, and thermal
14 variations, among others, can have a strong effect on the overall noise. Thus, while the
15 sensitivity of a device can be very high, the associated noise can lead to moderate LOD.
16 Moreover, for biosensing a receptor must be previously immobilized, and the
17 biofunctionalization protocol plays also a crucial role in achieving low detection limits. We
18 have chosen the limit of detection as the most suitable parameter for comparing the different IO
19 technologies. Two main ways of specifying the limit of detection can be employed: (i)
20 according to the bulk sensitivity (expressed as refractive index units (RIU) as all the evanescent
21 wave sensors are sensitive to any change in the bulk refractive index of the solution above the
22 sensor surface; (ii) according to the surface sensitivity, as the evanescent sensors are sensitive to
23 any accumulation of mass on the sensor surface, which is an evaluation of the real biosensing
24 capabilities of a transducer, normally expressed as surface mass density (pg/mm^2). Detection
25 limit can also be expressed as analyte concentration (i.e. in ng/mL or molarity), but this value is
26 not directly comparable among different sensors since it will depend on the target molecule and
27 its affinity constant. Best resolution for bulk refractive index changes (bulk sensitivity) are
28 within the range of 10^{-5} to 10^{-8} RIU, which depending on the analyte and transducer mechanism
29 means that concentration down to ng/mL or pg/mL can be determined.
30
31
32
33
34
35
36
37
38
39
40
41
42
43
44
45
46
47
48

49 Table 1 shows a comparison of the limits of detection (in RIU and pg/mm^2) for the integrated
50 optical sensors described along this review.
51
52

53 **3.1. Interferometric waveguide sensors**

54 Among the different integrated optical sensors, the interferometric ones are the most attractive
55 for biosensing due to their high sensitivity and broad dynamic range. Mach-Zehnder (MZI),
56 Young (YI) and Hartman interferometers are usual configurations employed for sensing (see
57 Figure 3).
58
59
60

In the integrated version of MZI, an input optical waveguide is split into two arms which after a certain distance are recombined again in an output optical waveguide (see Figure 3.A. for general structure and 3.B for a view of an integrated array of MZI). A biomolecular interaction in the sensor area within the evanescent field will produce a variation in the effective refractive index of the light propagating through this area, inducing a phase difference between the light travelling in the sensor and the reference arms. The interferometric modulation at the device output is described by:

$$I = \frac{I_0}{2} [E_S^2 + E_R^2 + 2E_S E_R \cos \Delta\Phi] \quad (1)$$

$$\Delta\Phi = \frac{2\pi L}{\lambda} [n_{eff,S} - n_{eff,R}] \quad (2)$$

Where E is the electric field propagating along the waveguide, n_{eff} is the effective refractive index, Φ is the phase, L is the detection length, λ is the light wavelength and I_0 and I are the light intensity at the input and output, respectively. The labels S and R stands for the sensing and the reference arm, respectively. An attractive aspect of this device is the possibility of using long interaction lengths, increasing the sensitivity. The optimization of the signal-to-noise ratio implies maximizing the transfer functions and hence maximizing all partial sensitivities (as could be $\partial\Delta\Phi/\partial n_{eff}$, etc) and, at the same time, minimizing all the perturbing effects, as could be temperature or wavelength drift. As can be deduced from equation (1), one main drawback of the interferometric sensors is that due to the cosine dependency, the sensitivity will depend on the position of the interferometric curve, with higher sensitivity at the quadrature points and strongly decreasing near the maximum or minimum of the curve. Modulation system should be an option in order to track the response to the quadrature position.

The main condition of an integrated interferometric device for biosensing application is the single mode behaviour of the waveguides. Each mode in a waveguide propagates at a different speed and its evanescent tail is different. Hence, if several modes, each one having a different sensitivity, simultaneously propagate in the waveguide, the information carried by them interferes, resulting in a decrease of the signal. For a fixed working wavelength, the modal properties of a guiding structure depend on the thickness of the waveguide core and on the refractive index contrast between the core and the surrounding media (claddings). To obtain single-mode waveguides, it is required to have a minimum difference between the refractive indices (RI) and/or a decrease of the waveguide dimensions. As a rule, if the difference between the RI of the core and the cladding is higher than 10%, single-mode can only be achieved with core thicknesses of hundreds of nanometers. In addition, for dense packaging of devices or for defining complex devices (as Mach-Zehnder interferometers), the waveguides must have 2D-

1
2
3 confinement, that is, light should remain confined in the cross-section. There are several
4 possibilities to achieve this confinement, but the most commonly employed is to partially etch
5 the waveguide core forming a rib which confines the light in the transversal direction. A careful
6 design of the rib is required to avoid excitation of lateral modes. As an example, for high index
7 contrast waveguides (as for example $\text{Si}_3\text{N}_4/\text{SiO}_2$), the rib should not exceed several nanometers
8 in depth to assure single mode behavior.
9

10
11
12
13
14 Glass-based [29-32] and polymer-based MZ interferometers using NOA81 [33] or SU-8 resist
15 [34], have been fabricated, and even assessed for biosensing purposes [35] with promising
16 results. Recently, Crespi et al. have reported the fabrication of a 3D MZI inscribed in a fused
17 silica chip with a previously fabricated microchannel, by using femtosecond laser writing [32].
18 However, in spite of the compactness and the high integration reached, the extrapolated LOD is
19 only of $1.5 \cdot 10^{-4}$ RIU, and no biosensing results have been reported. Most common MZ
20 interferometers are based on silicon nitride as core layer and silica as cladding. Initial works
21 with silicon-based MZI were addressed to optimize the structure and to improve the sensitivities
22 for biosensing applications [36-40]. Two different configurations, one based on total internal
23 reflection (TIR-based MZI) [37,41] and another one based on anti-resonant reflecting optical
24 waveguide (ARROW-based MZI) [42,43] have been proposed.
25
26
27
28
29
30
31
32
33

34 For TIR waveguides using silicon-related materials, maximum surface sensitivity and single
35 mode behavior are achieved for high refractive index contrast and core thicknesses of hundreds
36 of nanometers. The reported sensor has a core waveguide layer of 250 nm (Si_3N_4 , $n=2.00$), a
37 width of 4 μm and a rib of 3 nm, over a SiO_2 ($n=1.46$) cladding layer of 2 μm . The device is
38 covered with a protective SiO_2 layer except for the sensor area, to bring the waveguide into
39 contact with the environment [41]. Bulk sensitivity for a device with a sensor window of 15 mm
40 showed a limit of detection of refractive index of $8 \cdot 10^{-6}$ RIU, which corresponds to a surface
41 sensitivity of around $2 \cdot 10^{-4}$ nm^{-1} . Preliminary biosensing measurements based on antigen-
42 antibody interactions showed the feasibility of the device. Further biosensing real time
43 experiments of DNA hybridization reached detection levels of target complementary DNA of 10
44 pM with, high specificity as compared to control sequences [44] which means an extremely
45 high surface mass LOD of 0.06 pg/mm^2 .
46
47
48
49
50
51
52
53

54
55 An ARROW-based MZI was also developed [43]. In this case, the optical confinement of light
56 is based on antiresonant reflections rather than total internal reflections; these waveguides
57 exhibit low losses and permit larger dimensions (micrometers instead of nanometers) for
58 achieving single mode behaviour. An optimized structure with a core layer (SiO_2 , >2 μm
59 thickness, $n_{\text{core}}=1.485$), a second cladding layer (SiO_2 , 2 μm , $n=1.46$) and a first cladding layer
60

(Si₃N₄, 120 μm thickness, n=2.00) was fabricated. The rib depth was 60% of the core thickness and the waveguide width should have to be lower than 8 μm to obtain single-mode behavior [45]. Initial refractive index detection limit of 2.5·10⁻⁵ RIU was obtained [45], further improved to 2.5·10⁻⁶ RIU [46]. The device was also evaluated as immunosensor for the detection of an insecticide, carbaryl, by using a competitive immunoassay [46].

Young Interferometer (YI) is another well-explored interferometric device for biosensing. The YI is a waveguide with an integrated Y-junction acting as a beam splitter and, contrary to the MZI, the two beams are not recombined again. The exiting light from both arms is projected onto a CCD camera giving an interference pattern. When a biomolecular interaction takes place on the sensing arm, it induces a variation in the effective refractive index in this arm respect to the reference one ($n_{eff,S} - n_{eff,R}$). The phase difference of the two interfering rays is given by:

$$\Phi = \frac{2\pi}{\lambda} \left(\frac{d \cdot x}{f} - (n_{eff,S} - n_{eff,R}) \cdot L \right) \quad (3)$$

where d is the distance between the two branches, f is the distance between the output sensor and the read-out camera and x denotes the position on the camera. As an output, the fringe pattern moves laterally. One disadvantage of the YI device is the distance required from the output to the detector in order to get a maximum resolution. Advantages of the YI include the simplicity of the arrangement, the detection of the complete intensity distribution and the identical length of the arms which avoids side effects arising from temperature and wavelength drifts.

Brandenburg *et al.* [47,48] developed a free-space YI based on 154 nm thick Ta₂O₅ waveguide with single mode behavior. In this configuration, two separate beams are coupled into the sensing chip via a grating coupler. After propagating through the channels, light from both beams are coupled out by a second grating and diffracted by a double slit. The interference pattern is monitored on a CCD camera. A detection limit based on adsorbed molecules on the surface reached values of 0.75 pg/mm² and a resolvable variation of effective refractive index of 9·10⁻⁸ RIU [47]. Using this device, two different monoclonal antibodies have been immobilized on both channels and the specificity has been monitored together with the influence of samples diluted in complex matrices such as blood [49]. A careful study of an immobilization procedure based on the non-covalent deposition of bilayers of antibodies was followed, which guaranteed the absence of adsorption of interfering substances when spiked blood samples were added. Although the sensitivity levels were not studied in depth, it was possible to detect a low molecular weight substance as methotrexate in a direct way. By incorporating a two-channel fluidic cell (3 μL volume) for the reference and the sensing arm, the monitoring of recombinant

1
2
3 protein production was attempted [50]. A methodology based on the immobilization onto a
4 streptavidin modified surface of biotinylated antibodies, which recognize a tag introduced
5 during the protein expression process, was carried out showing a LOD around 50 ng/mL. This
6 LOD slightly increases up to 350 ng/mL when cell lysate was used instead of buffer (as this is
7 the real media from which the produced protein is extracted). Moreover, the viability of the
8 device for clinical diagnostics was demonstrated by the detection of tuberculosis-specific
9 antibodies in undiluted serum samples from infected patients [51]. A YI based on Ta₂O₅ planar
10 waveguide (150 nm thick) with integrated gratings for in and out coupling of the light, and with
11 a PDMS flow cell mounted on top, showed bulk detection limit of 5·10⁻⁶ RIU and DNA
12 hybridization sensing of 50 nM [52].

13
14
15
16
17
18
19
20
21 Ymeti *et al.* have developed a four-channel integrated Young interferometer [53] that enables
22 direct independent measurements in each sensing area, including one taken as a reference
23 (Figure 3.C). The refractive index resolution was close to 8.5×10⁻⁸ RIU (corresponding to an
24 estimated protein mass coverage resolution of 20 fg/mm²) [54] which is one of the most
25 sensitive values so far reported. With this design it was possible to correct and reduce by ten
26 times the temperature or setup drift. Moreover, the integration with microfluidics has reduced
27 the sample volume and the analysis response time, opening up the possibility to have a
28 miniaturized system. An immunoassay based on the immobilization of specific antibodies for
29 herpes simplex virus type 1 (HSV-1) detection was implemented with this device. Using one
30 channel as reference and the other one with an oriented antibody immobilization using protein
31 A, a limit of detection as low as 850 particles/mL was achieved, worsening when serum samples
32 were evaluated [55,56].

33
34
35
36
37
38
39
40
41
42 In the Hartman interferometer (Figure 3.D) a linearly polarized light is incoupled through
43 multiple sensing areas of an array of interferometers by using a grating fabricated onto the chip.
44 The viability of the platform for biosensing [57] was demonstrated by detecting levels of
45 hormones as low as 0.5 ng/mL in undiluted serum and blood samples, using an amplified
46 sandwich immunoassay [58,59]. An improved and more robust prototype integrating the laser
47 diode, the waveguides, the flow cell and the CCD camera was developed. The device showed a
48 LOD of 10⁻⁶ RIU and was recently used for the detection of avian influenza [60] by determining
49 the virus antigen (HA; hemagglutination antigen) with the specific antibodies covalently bound
50 onto the sensing channel.

51
52
53
54
55
56
57
58
59
60
61
62
63
64
65
66
67
68
69
70
71
72
73
74
75
76
77
78
79
80
81
82
83
84
85
86
87
88
89
90
91
92
93
94
95
96
97
98
99
100
101
102
103
104
105
106
107
108
109
110
111
112
113
114
115
116
117
118
119
120
121
122
123
124
125
126
127
128
129
130
131
132
133
134
135
136
137
138
139
140
141
142
143
144
145
146
147
148
149
150
151
152
153
154
155
156
157
158
159
160
161
162
163
164
165
166
167
168
169
170
171
172
173
174
175
176
177
178
179
180
181
182
183
184
185
186
187
188
189
190
191
192
193
194
195
196
197
198
199
200
201
202
203
204
205
206
207
208
209
210
211
212
213
214
215
216
217
218
219
220
221
222
223
224
225
226
227
228
229
230
231
232
233
234
235
236
237
238
239
240
241
242
243
244
245
246
247
248
249
250
251
252
253
254
255
256
257
258
259
260
261
262
263
264
265
266
267
268
269
270
271
272
273
274
275
276
277
278
279
280
281
282
283
284
285
286
287
288
289
290
291
292
293
294
295
296
297
298
299
300
301
302
303
304
305
306
307
308
309
310
311
312
313
314
315
316
317
318
319
320
321
322
323
324
325
326
327
328
329
330
331
332
333
334
335
336
337
338
339
340
341
342
343
344
345
346
347
348
349
350
351
352
353
354
355
356
357
358
359
360
361
362
363
364
365
366
367
368
369
370
371
372
373
374
375
376
377
378
379
380
381
382
383
384
385
386
387
388
389
390
391
392
393
394
395
396
397
398
399
400
401
402
403
404
405
406
407
408
409
410
411
412
413
414
415
416
417
418
419
420
421
422
423
424
425
426
427
428
429
430
431
432
433
434
435
436
437
438
439
440
441
442
443
444
445
446
447
448
449
450
451
452
453
454
455
456
457
458
459
460
461
462
463
464
465
466
467
468
469
470
471
472
473
474
475
476
477
478
479
480
481
482
483
484
485
486
487
488
489
490
491
492
493
494
495
496
497
498
499
500
501
502
503
504
505
506
507
508
509
510
511
512
513
514
515
516
517
518
519
520
521
522
523
524
525
526
527
528
529
530
531
532
533
534
535
536
537
538
539
540
541
542
543
544
545
546
547
548
549
550
551
552
553
554
555
556
557
558
559
560
561
562
563
564
565
566
567
568
569
570
571
572
573
574
575
576
577
578
579
580
581
582
583
584
585
586
587
588
589
590
591
592
593
594
595
596
597
598
599
600
601
602
603
604
605
606
607
608
609
610
611
612
613
614
615
616
617
618
619
620
621
622
623
624
625
626
627
628
629
630
631
632
633
634
635
636
637
638
639
640
641
642
643
644
645
646
647
648
649
650
651
652
653
654
655
656
657
658
659
660
661
662
663
664
665
666
667
668
669
670
671
672
673
674
675
676
677
678
679
680
681
682
683
684
685
686
687
688
689
690
691
692
693
694
695
696
697
698
699
700
701
702
703
704
705
706
707
708
709
710
711
712
713
714
715
716
717
718
719
720
721
722
723
724
725
726
727
728
729
730
731
732
733
734
735
736
737
738
739
740
741
742
743
744
745
746
747
748
749
750
751
752
753
754
755
756
757
758
759
760
761
762
763
764
765
766
767
768
769
770
771
772
773
774
775
776
777
778
779
780
781
782
783
784
785
786
787
788
789
790
791
792
793
794
795
796
797
798
799
800
801
802
803
804
805
806
807
808
809
810
811
812
813
814
815
816
817
818
819
820
821
822
823
824
825
826
827
828
829
830
831
832
833
834
835
836
837
838
839
840
841
842
843
844
845
846
847
848
849
850
851
852
853
854
855
856
857
858
859
860
861
862
863
864
865
866
867
868
869
870
871
872
873
874
875
876
877
878
879
880
881
882
883
884
885
886
887
888
889
890
891
892
893
894
895
896
897
898
899
900
901
902
903
904
905
906
907
908
909
910
911
912
913
914
915
916
917
918
919
920
921
922
923
924
925
926
927
928
929
930
931
932
933
934
935
936
937
938
939
940
941
942
943
944
945
946
947
948
949
950
951
952
953
954
955
956
957
958
959
960
961
962
963
964
965
966
967
968
969
970
971
972
973
974
975
976
977
978
979
980
981
982
983
984
985
986
987
988
989
990
991
992
993
994
995
996
997
998
999
1000

Contrary to previous designs, in which two arms (a sensing and a reference one) are separated, a novel configuration based on interferometry but using a single waveguide has been recently developed. The so-called bimodal waveguides (BMWG) [61] is a single waveguide, with two

different zones: a starting one of single-mode behavior and a second-one which supports two modes (zero and first-order mode) which propagate at different velocities depending on the refractive index of the cladding layer (see Figure 3.E). The interference pattern at the exit of the waveguide changes if the refractive index varies, for instance, as a consequence of a biointeraction event. The configuration is significantly less complex than for conventional interferometers while the sensitivity level achieved is comparable (detection limit of $2.5 \cdot 10^{-7}$ RIU [61]). The sensing chip was fabricated onto a silicon substrate using standard microelectronics technology. A Si_3N_4 layer ($n=2.00$, thickness= 350nm) was deposited onto SiO_2 ($n=1.46$, thickness= $2\mu\text{m}$) and a ridge type waveguide (2 nm height) was formed on top by BHF etching. The single mode region was reduced to 150 nm thickness. The device is covered with a SiO_2 cladding layer. The initial design includes chips with dimensions of $30 \times 10 \text{ mm}^2$ and 26 independent interferometers. A preliminary immunosensing of human growth hormone has shown an excellent sensitivity of 30 pg/mL (*Lechuga et al., unpublished results*).

3.2. Grating coupled waveguide sensors

Grating-coupled waveguide sensors are one of the first transducers earlier developed [62,63]. A grating coupler is a system of periodic disturbance in a planar single-mode waveguide (commonly $\text{SiO}_2\text{-TiO}_2$ or Ta_2O_5). The grating allows the excitation of a guided mode of the waveguide at a certain angle of incidence when the incoupling condition is fulfilled:

$$n_{\text{eff}} = n_{\text{air}} \sin \alpha + l \left(\frac{\lambda}{\Lambda} \right) \quad (4)$$

Where n_{eff} is the effective refractive index of the waveguide, n_{air} is the refractive index of air, α is the angle of incidence of the light, l is the diffraction order, λ is the wavelength and Λ is the grating period. As can be deduced from equation (4), the incoupling angle is sensitive to any variation in the refractive index at the surface of the waveguide (n_{eff}) within the evanescent field region. Therefore, induced changes in the coupled angle can be used for sensing. Conversely, it is possible to evaluate the outcoupling angle of the guided light.

In the input grating coupler device, s- and p- polarized laser beams are scanned at a variable angle to excite both TE and TM modes. The grating sensor requires a precise mechanical movement of the rotation stage which includes the sensing platform, the fluidics and the photodetectors [64,65]. On the other hand, output grating devices are based on the monitoring of the outcoupling angle, which does not require a moving stage, simplifying the setup and decreasing the response time [66,67]. The in- and output grating configurations were initially developed by Nellen and Lukosz in the early nineties, showing a refractive index LOD around 10^{-6} RIU. Some initial biosensing evaluations using model systems as IgG/antiIgG or

1
2
3 biotin/streptavidin showed moderate sensitivities. Years later, more in depth biosensing
4 experiments were demonstrated such as competitive immunoassays [68,69], on-line monitoring
5 of monoclonal antibodies production [70], the influence of surface biofunctionalization [71] or
6 the determination of kinetics rate constants [72]. A new setup configuration based on reflection-
7 mode operation avoiding any moving part was developed by Brandenburg *et al.* [73], which
8 considerably simplified the previous one. The incident polarized light is focused on the grating
9 by a lens in such a way that all the coupling angles in the expected range are included, and the
10 minimum of the reflected light is followed by a CCD camera. A similar bulk LOD ($3 \cdot 10^{-6}$ RIU)
11 was reached and some biosensing experiments based on competitive immunoassays were
12 reported, as pesticide detection [74], optimization of surface biofunctionalization [49] or DNA
13 hybridization [75,76].

21
22
23 More recently, Grego *et al.* [77] have used silicon oxynitride (SiO_xN_y) deposited by plasma-
24 enhanced chemical vapor deposition (PECVD) to improve the performance of a grating coupled
25 sensor. Two technologies, colloidal self-assembly and imprint lithography were used in order to
26 incorporate the gratings on the waveguide. With the last one, two dimensional grating structures
27 with optimum pitch in two orthogonal directions were designed and tested in input grating
28 coupler configurations by angular and wavelength interrogation [78]. This 2D structure showed
29 a sensitivity enhancement (a factor of two) as compared with conventional one-dimensional
30 grating sensor. [79]. Yuen and coworkers [80] have developed a self-referencing optical
31 detection system, by using novel microfluidics which efficiently divides the grating in two
32 halves. The grating operates under reflection mode, and the CCD image obtained can be
33 processed to analyze the separate responses.

41
42 Wiki *et al.* [81,82] developed the so-called WIOS (Wavelength Interrogated Optical Sensor),
43 based on grating couplers (Figure 4.A). The approach is based on a single mode waveguide
44 structured with two grating couplers, to in and out-coupling the light, respectively. The change
45 of the refractive index due to an interaction onto the surface is monitored by scanning the
46 resonance peak at a fixed angle of incidence by a tunable laser diode and adjusted with a mirror.
47 The emitted light is collected by a multi-mode fiber and detected by photodiodes. In order to
48 have different in and out coupling angles, two different grating configurations were designed,
49 one with a grating with different periods for in and output and the other one based on a single
50 grating with different thickness layer (see Figure 4.A). Reference pads close to sensing pads are
51 also included for self-referencing, thus improving the signal-to-noise ratio. A compact device
52 including four channels and the laser source, the mirror, the flow cell and other components was
53 also developed and tested for biosensing of low molecular weight analytes, such as biotin, and
54 large biomolecules, such as antibodies, showing mass detection limits of 0.3 pg/mm^2 . The

1
2
3 device showed a label-free detection of molecules as small as 200 Da. Further development of
4 this integrated device has improved its multiplexed capabilities by using chips with up to 24
5 different sensing areas (each one with the input and output gratings). Adrian *et al.* [83] have
6 applied the device with a flow cell of three 7.2 μL channels for the detection of sulfonamides, a
7 family of antibiotics widely used in veterinary medicine as feed additives. The test was based on
8 indirect immunoassays where the antigen was covalently immobilized onto the chip surface
9 previously functionalized with a photopolymerizable dextran layer for avoiding non-specific
10 interactions. A limit of detection in milk samples of 0.5 $\mu\text{g/L}$ was achieved but an additional
11 amplification step with a secondary antibody was required. The multiplexed capabilities of the
12 device were tested for the simultaneous detection of four different families of antibiotics [84].
13 By following a similar protocol as above, four different antigens were spotted in separate
14 sensing areas. The multi-assay, with capability to detect 34 antimicrobials, was done in milk
15 sample showing the same sensitivity with high levels of specificity, indicating the potential of
16 the sensor as a screening analytical tool. The combination of the WIOS configuration with a
17 polymer-based self-contained microfluidic cartridge [85] has added more value to the sensor as
18 a lab-on-a-chip device to be employed at the agroalimentary industry (Figure 4.B). Semi-
19 quantitative assays for the simultaneous detection of three different antibiotic families have been
20 developed. Pasche *et al.* simultaneously detected three different cytokines using a sandwich
21 immunoassay [86] and the sensor was also tested in cell cultures for studying inflammatory
22 processes by the quantification of cytokines released by the cells. In the field of genomics, it has
23 been employed to study the kinetics of covalent immobilization of double-stranded
24 oligonucleotides in order to evaluate the optimal hybridization efficiency after sequential
25 denaturation [87].

3.3 Ring Resonator sensors

42 Ring resonator transducers are increasingly being used for biosensing due to their high
43 sensitivity and their potential to be produced in highly dense arrays for multiplexed analysis. In
44 a ring resonator configuration, light is coupled by an input waveguide via the evanescent field
45 into a circular waveguide. Coupled light propagates through the loop in the form of whispering
46 gallery modes in such a way that constructive interference is generated in the multiple round-
47 trips over the ring circumference, considerably enhancing the sensitivity. Detection in a ring
48 resonator is based on a refractive index change, which is related to the WGM spectral position
49 through the resonant condition:

$$\lambda = 2\pi n_{\text{eff}} r / m \quad (5)$$

50 where m is an integer describing the WGM angular momentum, λ is the wavelength; r is the
51 radius of the ring and n_{eff} is the effective refractive index experienced by the WGM. A change in
52
53
54
55
56
57
58
59
60

1
2
3 the effective refractive index of the ring environment due to biointeractions onto the ring surface
4 shifts the resonance spectrum, which can be monitored by scanning the wavelength or by
5 measuring the intensity profile at a fixed wavelength.
6
7

8
9
10 Contrary to straight waveguides, in ring resonators interaction is not longer determined by the
11 length of the waveguide but rather by the number of revolutions within the ring, which is
12 indicated by the resonator quality factor (Q factor). The effective length (L_{eff}) is related to the Q
13 factor by:
14

$$L_{eff} = Q\lambda/2\pi n \quad (6)$$

15
16
17
18
19
20 Where λ is the wavelength and n the refractive index of the ring resonator. High Q factors
21 indicate low optical losses and long photon lifetimes, which is translated into narrow line-
22 widths and high peak resolution (which means a high sensitivity). Relatively high Q factors of ~
23 10^6 can be achieved in resonators of few μm (typically around 50-200 μm), which is equivalent
24 to have planar waveguides of several cm. For example, a quality factor of 10^8 means that the
25 molecule will be sampled more than 100.000 times [91]. Therefore, despite the small size of the
26 resonator, it could achieve higher sensitivities than straight waveguides while using orders of
27 magnitude less surface area. That is the reason why these devices can be subjected to a high
28 degree of integration.
29
30
31
32
33

34
35
36 Few types of integrated optical-based resonating structures have being explored for biosensing,
37 as the planar microring resonators based on microdisks [88-91], microrings [92-97], or
38 microtoroids [98-102]. Compact ring resonators with optimal photonic properties and optimal
39 sensitivity can be fabricated (see Figure 5) including complex configurations incorporating
40 multiple resonators. Different materials such as glass-based [103,104], $\text{Si}_x\text{N}_y\text{-SiO}_2$ [105] or
41 polymer-based [106-109] ring resonators have been reported and applied to DNA, proteins or
42 bacteria detection [104] (Figure 5.A.). Recently special attraction is gaining silicon-on-insulator
43 (SOI)-based resonators [110]. De Vos *et al.* [92] have described SOI microring resonators (5 μm
44 radius, Q factor of 20,000) with a bulk refractive index sensitivity of 70 nm/RIU, which
45 corresponds to a minimal detectable refractive index shift of 10^{-5} RIU. Biosensing evaluation of
46 avidin interaction onto a biotinylated surface led to estimated detection limits around 10 ng/mL
47 [92,111], which is comparable to other label-free sensors. Recently, the same group has reported
48 an array of SOI microring resonators [112] based on three series of four rings connected to a
49 single input waveguide, one for each series, and each one with individual output waveguides
50 (Figure 5.B.). The incoming and outgoing light is coupled by grating couplers and the
51 collected signal of the twelve resonators is imaged on an infrared camera. The four resonators in
52
53
54
55
56
57
58
59
60

1
2
3 each series have different circumference ratio (with variations about 30 nm) showing
4 independent and not overlapped resonance spectra. A PDMS flow cell with independent
5 microfluidic channels ($200 \times 50 \mu\text{m}^2$) was mounted on top of the chip for sample delivery. The
6 multiplexed capabilities were evaluated by immobilizing three different proteins and by
7 successively flowing two of the three specific antibodies. Due to the optimized surface
8 biofunctionalization, the device showed high specificity and low non-specific adsorption (which
9 could be also corrected by one resonator acting as reference) [111]. With an estimated peak
10 resolution around 0.4 pm and a Q factor around $2 \cdot 10^4$, a surface mass detection limit resulted in
11 3.4 pg/mm^2 .
12
13
14
15
16
17

18
19 Li *et al.* [94] proposed a two concentric ring structure in order to increase the notch depth and
20 the sensing area at the same time. The sensor was fabricated over a SOI wafer with an outer
21 radius of 21 μm , and an inner radius of 20 μm , and an air gap of 480 nm between them, coupled
22 to a waveguide of 10 μm width tapered down to 480 nm. The estimated Q factor of this
23 resonator was around $5.1 \cdot 10^4$ and bulk sensitivity was considerably high, of 683 nm/RIU. Iqbal
24 *et al.* [96] have recently developed a biosensing platform based on the integration of 32 ring
25 resonators accessed via a bus waveguide, which are simultaneously interrogated (Figure 5.C.).
26 24 of them are used as sensing resonators, with an etched window on the surface for sample
27 interaction, whereas the reminding eight, left under the cladding layer, are used as reference for
28 temperature-induced drift. Light is coupled in and out by grating couplers. The chip is covered
29 with a flow cell that comprises the fluidic ports, channels, and reservoirs for fluid delivery to the
30 32 sensors by using gaskets that define the channels in each sensing area. The optical setup is
31 complex but allows simultaneous reading of 24 interactions. A RI detection limit of $7.6 \cdot 10^{-7}$ was
32 achieved [96], with good repeatability among the different resonators and an estimated surface
33 LOD of 1.5 pg/mm^2 [97]. AntiIgG/IgG and biotin/streptavidin interactions were used as proof-
34 of-concept systems in order to assess the biosensing capabilities, and a preliminary real-time
35 multiplexed analysis of DNA hybridization showed the viability of the device [96]. From the
36 strict biosensing point of view, this platform has been applied few times for in-depth
37 bioanalytical problems. For instance, by immobilizing specific antibodies [113], cytokines have
38 been detected at low concentrations (below 0.1 ng/mL in buffer) [114] but incorporating a
39 secondary antibody for amplification of the signal. A sandwich assay was applied to the
40 detection of cellular secretion of cytokines, showing the viability of measuring them in cell
41 culture media, while retaining the sensitivity. Moreover, regeneration of the antibody layer was
42 achieved, a step not always contemplated in experiments with biosensors. The use of several
43 microrings ($n=15$) diminishes the uncertainties, and increases the reliability of the tests.
44 Similarly, it has been detected a cancer biomarker by immobilizing the specific antibodies for
45 carcinoembryonic antigen (CEA) in a single microring [115] achieving a detection limit around
46
47
48
49
50
51
52
53
54
55
56
57
58
59
60

1
2
3 25 ng/mL in a complex media like serum, which is close to relevant diagnostic concentrations.
4 The multiplexed capabilities of the arrayed resonators were evaluated by immobilizing six
5 different antibodies (five specific antibodies and one non-specific as control, four microrings for
6 each one, see Figure 5.C.) for the multiplexed determination of five relevant proteins. Prostate
7 specific antigen (PSA), α -fetoprotein (AFP), carcinoembryonic antigen (CEA), α -tumor necrosis
8 factor (TNF- α), and interleukin-8 (IL-8) were simultaneously detected in an unknown protein
9 cocktail solution [116]. A fast (10 min), sensitive (<150 fmol) and simultaneous detection of
10 multiple micro RNAs (miRNAs) using single strand DNA as immobilized probes onto the
11 microring array (four different sequences) has also been recently published [117]. Single
12 nucleotide polymorphism could even be discriminated and expression levels of miRNA in cells
13 were also determined.
14
15
16
17
18
19
20
21

22
23 Toroidal-shaped based microcavities offer resolution levels significantly higher than previous
24 structures, since they exhibit ultrahigh Q factors ($>10^8$) [118,119] while preserving the same
25 advantages for mass production and integration capabilities as planar ring resonators.
26 Microtoroids can be fabricated in arrays over silicon wafer using standard lithography
27 techniques (see Figure 5.D.) with dimensions ranging from 30 to 150 μm for the major diameter
28 to 2.5-6 μm for the minor diameter. The structures are coupled to a low-loss tapered optical
29 fiber and have been evaluated for biosensing by immobilizing specific antibodies using protein
30 G for oriented attachment. With this configuration, cytokines were detected at extremely low
31 levels, with a LOD around 5 aM ($5 \cdot 10^{-18}$ M), showing a wide working range of around 12 orders
32 of magnitude in buffer conditions and with the remarkable capability of resolving single
33 molecule detection [98]. The capabilities of the sensor were also evaluated in 10-fold diluted
34 serum. The same group has attempted the fabrication of low-loss polymer [99] or polymer-silica
35 hybrid [120] toroids, which, even with a lower Q factors (10^5 - 10^7), are still significantly
36 competitive with other ring resonators. Nevertheless their biosensing capabilities have not been
37 shown yet.
38
39
40
41
42
43
44
45
46
47
48

49 3.4. Photonic crystal waveguide sensors

50 Photonic crystal-based biosensors are a relatively novel technology which is gaining much
51 attention and is growingly appearing in literature [121,122]. Photonic crystals are well defined
52 nanostructures with periodically repeated variations in the refractive index in one, two or three
53 orthogonal directions generating one, two or three dimensional photonic crystals (1D, 2D or 3D
54 PhC). The lattice structure is generated on the length scale of the light wavelength, which
55 generates photonic bandgaps where light cannot propagate in the crystal. The width and position
56 of the photonic gap is highly dependent on the refractive index change between the dielectric
57 materials and on the periodicity of the structure [123], which is exploited for sensing.
58
59
60

1
2
3
4
5 Integrated photonic crystals have been interestingly applied in dielectric mirrors, lasers,
6 narrowband optical filters, microresonators and in waveguide structures and due to their high
7 degree of integration they are ideal candidates for lab-on-chip biosensing. Device structures
8 based on linear gratings and 2- dimensional gratings (i.e. arrays of holes arranged in
9 checkerboard or hexagonal close-packed grids along the sensor surface) are the simplest ones in
10 terms of fabrication and sensing. The introduction of discrete or line defects on the grating
11 structure generates transducer cavities with enhanced sensitivity. The strong confinement of the
12 light in the periodic lattice makes these materials very attractive not only because of the
13 sensitivity but also due to their small dimensions, limited to few μm^2 , which allows for low
14 sample consumption.
15
16
17
18
19
20
21

22
23 Cunningham's Group has pioneered the development of bulk photonic crystal based biosensors.
24 [124-126]. They have implemented a one-dimensional subwavelength polymer grating coated
25 with a layer of high refractive index (TiO_2) [127]. White light is perpendicularly impinged on
26 the sensor surface and the reflected light is collected, which shifts after a biomolecular
27 interaction takes place. The fabrication has been implemented into continuous sheets of plastic
28 films. The interrogation method can read individually several areas of the surface, avoiding
29 optical crosstalk between adjacent sensor regions. The overall technology offers the possibility
30 to produce low cost, disposable sensing surfaces with high throughput capabilities [128]. In
31 addition, the sensing surfaces have been adapted to be allocated at the bottom of microtiter
32 plates (96, 384 or 1536 formats) [128] or microarray slides [128]. Moreover, they can be
33 integrated within microfluidic networks by replica molding of the photonic crystal sensors and
34 fluid channels in a simultaneous process [129-131]. The latter configuration permits kinetic and
35 high resolution endpoint spatial measurements, improving the detection time and decreasing the
36 detection limit as compared to standard in-well detection [132]. Recently, a microfluidic array
37 chip with combinatorial mixing and on-chip sensing capabilities has also been demonstrated
38 using AtC (Actuate to Close) microfluidic networks [133]. The sensors have been exploited for
39 a wide range of bioassays [134], including cell-based assays, characterization and study of cells
40 attachment to surfaces [135-137], protein and virus detection [132] [138], study of small
41 molecules aggregation for drug screening [139], or for protein-protein interactions [140], among
42 others. The technology based on standard microplate-based assays has been commercialized by
43 SRU Biosystems (www.srubiosystems.com) (see Section 4).
44
45
46
47
48
49
50
51
52
53
54
55
56
57

58 Photonic crystals with a defined structure can offer interesting alternatives. Beside few
59 examples, such as a pillar-based array of 2D photonic crystals [141] recently developed but not
60 evaluated for biosensing, most of the work is focused on hole-array PhC (see Figure 6.A.).

1
2
3 Planar photonic waveguides, where a guided wave is generated by missing holes or defects in
4 the bulk photonic crystal structure have been fabricated on SOI wafer. Unfortunately, and
5 despite the large effort invested, scarce biosensing examples can be found in the literature and
6 such examples are only at the proof of concept level. Most of the work is mainly focused on
7 fabrication, simulation experiments and bulk refractive index evaluation to establish the
8 sensitivity of the structures.
9

10
11
12
13
14 Some examples are worthy to be mentioned as the work by Dofner *et al.* who designed and
15 fabricated a SOI photonic crystal waveguide consisting of a hexagonal lattice of holes with a
16 single missing row line defect and point cavities in different arrangements (either a defect based
17 on three missing holes, a single hole or a shifted line of holes arranged perpendicular to the
18 waveguide orientation) (see Figure 6.A. bottom)[142,143]. The optical properties of all the
19 structures were assessed by TE polarized light coupled in and out of the ridge waveguide by a
20 tapered fiber, allowing in-planar-geometry evaluation. By placing a flow cell on top of the
21 structure, refractive index sensing in the most optimal case (Q factor ~3000) gave a bulk LOD
22 of $\sim 10^{-3}$ RIU [142]. Surface sensitivity was assessed by physisorption of BSA or avidin as
23 model proteins, giving a mass sensitivity around 24.7 nm/pg, with a minimal detectable mass of
24 around 4 fg and a detection limit of ~ 500 pg/mm².
25
26
27
28
29
30
31
32

33
34 Skivesen *et al.* [144] have fabricated a waveguide with holes of 240 nm in diameter, a lattice
35 constant of 370 nm and a length of 25 μ m, using electron-beam lithography and inductively
36 coupled plasma etching. A BSA adsorption was demonstrated under static conditions. A similar
37 structure has been used for protein and DNA sensing [145,146]. The photonic crystal length was
38 20 μ m with a lattice constant and hole radius of 390 and 111 nm, respectively. A 500 nm wide
39 single-mode access waveguide was employed to obtain a sharp band edge (see Figure 6.A). A
40 LOD of $6 \cdot 10^{-4}$ RIU was achieved [145]. Tapered fibers were used for the in- and outcoupling of
41 TE polarized light and a flow cell was mounted on top of the sensing surface. Hybridization of
42 DNA strands was monitored in the nM range [146]. For proteins, anti-BSA was detected over a
43 BSA-functionalized surface, reaching a mass detection limit of 2.1 pg/mm² (which means a total
44 mass detection limit of 0.7 fg).
45
46
47
48
49
50
51
52

53
54 1D photonic crystal microcavities fabricated by x-ray lithography on SOI wafer have also been
55 described [147], introducing defects in the structure by breaking the periodicity of the holes.
56 The resonant wavelength can be tuned according to the defect cavity spacing. This type of
57 structure has been adapted by Erickson's group for the development of the so-called Nanoscale
58 Optofluidic Sensor Array (NOSA). This sensor has a microcavity structure (resonator) that is
59 evanescently coupled to an adjacent single-mode silicon waveguide. The design of the structure
60

1
2
3 includes parallel resonator arrays with slightly different cavity spacing and, therefore, different
4 resonant wavelength and with individual Q factors between 1000 and 3000, all of them placed
5 along a single waveguide (see Figure 6.B.). Nanotapers were used for light coupling and a
6 PDMS flow channel running orthogonally to the array was mounted onto the chip, for
7 simultaneous and multiplexed detection [148]. Bulk refractive index LOD of $7 \cdot 10^{-5}$ RIU was
8 experimentally determined, which could be translated into a high sensitivity for mass detection,
9 when considering the extremely high confinement in the inner holes. Detection of serotypes of
10 Dengue virus was demonstrated by immobilizing four different DNA probes in different
11 resonators and subsequently adding the specific DNA target for one of them [149]. These
12 experiments only showed a proof-of-concept for nucleic acid interaction. Similarly,
13 immunochemical multiplexed detection of interleukins (IL) was also addressed [150]. Three
14 different specific antibodies for IL4, 6, and 8, respectively, were immobilized and a sandwich
15 assay was performed by adding the target followed by a secondary specific antibody in order to
16 enhance the signal. It is worth noticing that the device has low sensitivity since it has moderate
17 Q factors (3000), which may be enhanced by optimizing the crystal structure (such as the gap
18 and hole dimensions). Although the sensitivity of this PhC sensor is not high, this is one of the
19 few examples showing biosensing capabilities while including a multiplexed configuration.
20
21
22
23
24
25
26
27
28
29
30
31

32 Fauchet *et al.* have also made a strong contribution in this area by developing two dimensional
33 photonic crystal-based structures [151]. Biotin-streptavidin interaction and covalent
34 immobilization of BSA were evaluated and a minimum mass coverage of around 2.5 fg was
35 detected [151]. SOI-based wafers were used to fabricate photonic crystal waveguides with a
36 defect line in the structure to guide the light. Recently, a structure where the defect line is
37 generated adjacent to the photonic microcavities has been proposed in such a way that the
38 device can operate as a multi-channel sensor [152,153]. This structure shows a limited
39 sensitivity with Q factors around 400 and bulk LOD in the range of 10^{-2} RIU. Biosensing
40 evaluation was done under static regime, with incubation steps and evaluation in dry
41 environment. The surface was covalently modified with antibodies (anti-IgG) and target
42 antibodies (IgG) were detected, observing a detection limit around 67 nM (10 μ g/mL) which
43 corresponds to a surface sensitivity of $2.3 \cdot 10^5$ nm/M [153]. Considering that the major
44 contribution to the signal comes from the most sensitive area of the region (the defect in the
45 structure and the surrounding holes) a surface density of 1 ng/mm² and a minimum mass of 1.5
46 fg could be detected.
47
48
49
50
51
52
53
54
55
56
57

58 Zlatanovic *et al.* designed a photonic crystal (Figure 6.C) structure with a ridge waveguide but
59 with low Q factors (around 400) [154]. Real time biosensing was demonstrated by immobilizing
60 biotin-BSA and detecting specific antibodies against biotin. An excellent limit of detection of

1
2
3 20 pM of antibody was achieved, which in terms of mass and considering the affinity of the pair
4 antibody/antigen was found to be around 4.5 fg. Moreover the experiments included the
5 regeneration of the bioactive surface. These results demonstrated that despite the low resolution
6 of the device (due to the low Q factor), an adequate biofunctionalization of the surface could
7 lead to acceptable sensitivities for biodetection.
8
9

10
11
12 Overall, photonic crystal structures still remain as a promising type of transducers with
13 moderate sensitivities as compared with other label free photonic sensors. Better features could
14 be achieved by optimizing the crystal and defect dimensions and also by positioning the
15 bioreceptor only in the holes (by controlled immobilization), where the confinement is
16 maximum, therefore resulting in highest resonant shifts. In fact, a growing number of examples
17 are appearing in the literature focused on single particle detection by trapping them at the holes;
18 single virus or small pathogens could be detected in this way [155-157].
19
20
21
22
23
24
25

26 **3.5. Silicon wires, slot waveguides and other nanophotonic sensing configurations**

27 In this section we include an overview of the new and emerging trends in the design and
28 implementation of nanophotonic structures for sensing, which we envisage could be highly
29 competitive with the ones described in previous sections, either due to their sensitivity or to
30 their capabilities towards integration and miniaturization. Among them, slot waveguide-based
31 structures and silicon wires stand out for their potential enhanced sensitivity due to the
32 confinement of the electromagnetic field and for their highly integration capabilities in compact
33 dense arrays of individual sensors with versatile geometries. Unfortunately, few biosensing
34 experiments have been demonstrated with these devices, and only proof-of-concept experiments
35 with model systems have been published so far.
36
37
38
39
40
41
42

43 Silicon photonic wires are submicron channel waveguides fabricated by electron beam
44 lithography and reactive ion etching on SOI wafers. The high index contrast between the silicon
45 core ($n=3.5$) and silica cladding ($n=1.5$) yields a strong field confinement and allows for sharp
46 waveguide bends radii of few microns with low losses. With this technology the fabrication of
47 waveguides with higher compactness and higher intrinsic sensitivity (provided by the TM
48 mode) than the lower-contrast index material counterparts is possible. Initially developed for
49 optical switches, directional couplers and other telecommunications applications, silicon wires
50 first showed up in the biosensing field by the pioneer work of Janz's group. This group first
51 described a Mach-Zehnder interferometer based on SOI photonic wire waveguides [158] and a
52 double spiral millimeter-long resonator folded within a compact size of 100-150 μm (and a Q
53 factor of 17600) (Figure 7.A.). Both sensors were fabricated on SOI wafer with a Si core
54 thickness of 0.26 μm and a buried SiO_2 cladding of 2 μm . Single mode wire waveguides of 450
55
56
57
58
59
60

1
2
3 nm width were selected and a SU-8 cover layer was employed to isolate the non-sensing
4 regions. Bulk sensitivity and surface biomolecular interactions were evaluated under flow
5 regime (using a PDMS microflow cell). Updated versions incorporate improvements such as a
6 reference arm to suppress wavelength and temperature drift [159,160], integration of dense
7 arrays of six spiral MZI with an SU-8 fluidic channel for the delivery of liquids [161], or the use
8 of four resonators [162], which overall opens up the possibility to perform multiplexed analyses
9 (see Figure 7.A.). The dimensions of the folded wires are suitable for a controlled surface
10 functionalization using conventional spotters. The performance of the sensing devices was
11 assessed by immobilizing two different antibodies in individual sensors and simultaneously
12 evaluating them with the corresponding anti-IgG. For the MZI configuration, TM polarized
13 light is delivered by an optical fiber which splits the light to the six sensors; parallel readout of
14 the light exiting the six output waveguides is done by a near infrared camera. Results have
15 shown the discrimination between the different biomodified surfaces, demonstrating the high
16 potential of silicon wires-based devices for multiplexed biosensing. However, results are not yet
17 conclusive about the sensitivity of these sensors and only estimated values of resolvable surface
18 coverage around 0.25 pg/mm^2 are theoretically predicted (corresponding to a detected molecular
19 mass of 0.5 fg) [161]. In the case of resonators, with radius between 20 and $28 \text{ }\mu\text{m}$ (and
20 improved Q factors of 25000) and a reference included in the structure, a bulk sensitivity of 135
21 nm/RIU ($<2 \cdot 10^{-6} \text{ RIU}$) has been achieved and a surface immunochemical detection down to 20
22 pM (resolvable mass of 40 ag) [162] has been shown so far.

23
24
25
26
27
28
29
30
31
32
33
34
35
36
37 Slot-waveguides [163-165] consist of two slabs of high refractive index materials separated by a
38 nanometer-scale low refractive index slot region and surrounded by low-refractive index
39 cladding materials in such a way that light is strongly confined in the slot region. A stronger
40 light-analyte interaction can be achieved within this region as compared to conventional rib or
41 planar waveguides, which results in an enhanced sensitivity. Moreover, slot-waveguides can be
42 fabricated within structures such as resonators or interferometers by employing CMOS
43 compatible materials and technology, including SOI technology, which enables miniaturization,
44 and further integration within lab-on-a-chip platforms.

45
46
47
48
49
50
51
52 So far, slot-waveguide resonators have been reported by only two research groups. Barrios *et al.*
53 pioneered the slot waveguide configuration, using $\text{Si}_3\text{O}_4\text{-SiO}_2$ for the fabrication of a slot-
54 waveguide ring resonator structure [166], with a radius of $70 \text{ }\mu\text{m}$ and slots of 200 nm for both
55 the waveguide and the resonator. A bulk sensitivity of 212 nm/RIU for a resonator with a Q
56 factor of 1800 was reached, significantly better than conventional resonators, indicating a
57 considerably contribution from the slot region. Biosensing evaluation was done off-flow by
58 covalently immobilizing antibodies onto the surface and detecting their specific target (in this
59
60

1
2
3 case BSA as model system) showing a surface limit of detection of 16 pg/mm^2 [167], which
4 indicates a poor to moderate sensitivity as compared to most of the optical biosensors (see Table
5 1 for comparison). Recently, a highly integrated chip based on an array of eight slot-waveguide
6 ring resonators (two references—one for laser alignment and compensation and another one for
7 control- and six for parallel analyses) have been fabricated [168], including the microfluidics
8 integrated with the sensor in a cartridge (40 mm x 15 mm) and the alignment with the read-out
9 instrumentation for simultaneous detection (see Figure 7.B). The incoming light is coupled by
10 fully etched surface grating couplers, and split by multimode interference splitters to all the
11 channels (reference and sensing ones included). The outcoupling is done by imaging the
12 waveguide end faces onto a photodiode array. Each sensing area is individually reached using a
13 single PDMS flow cell. Bulk detection limit was 5×10^{-6} RIU, similar to the one previously
14 reported for individual sensors, which is considerably good as compared to conventional
15 resonators or single slot sensing configuration. A surface mass detection limit of 0.9 pg/mm^2
16 was achieved, which is significantly better than previous values, mainly due to the use of
17 reference channels for compensation of temperature drifts, and to the use of a laser with smaller
18 wavelength step [169]. Claes *et al.*[95] adapted their work with conventional resonators to the
19 development of a SOI-based slot waveguide ring resonator. They simulated the optimum
20 dimensions of the photonic structure (slot and rib width) in order to obtain the maximum
21 resonance shift to make it feasible for biosensing. A ring resonator (5 μm bending radius) with a
22 104 nm slot width, 268 nm rib and 220 nm height, with two identical bus waveguides was
23 fabricated to get the maximum light coupling via single-mode fibers vertically coupled with
24 gratings. With this resonator, a four times better bulk sensitivity (298 vs 70 nm/RIU) was
25 reached as compared with conventional waveguide resonator.

26
27
28
29
30
31
32
33
34
35
36
37
38
39
40
41
42 Instead of ring structure with a vertical slot, Lee *et al.* [89,90] designed a horizontal air-slotted
43 silicon nitride microdisk resonator. In particular, 15 μm diameter microdisks were fabricated by
44 a multilayer deposition (240 nm SiN_x /40 nm SiO_2 /240 nm SiN_x) on a silicon surface and
45 selective wet etching. A further hydrofluoric acid etch of the SiO_2 defines a 2 μm deep
46 horizontal air slot from the disk edge with a thickness of 40 nm. In this way, it is possible to
47 obtain ultra-thin slots with high smoothness in the slot walls (see Figure 7.C) and an
48 enhancement of the sensitivity due to the spatial confinement in the slot region. Microdisks with
49 Q factors of ~ 7000 were obtained. By using a 1 μm tapered fiber to couple the light (TM mode)
50 in and out, surface sensitivity was evaluated by assessing the resonance shift of the fundamental
51 radial mode at various streptavidin concentrations added onto a disk previously modified with
52 biotin groups. A value of 2.5 nm/ $(\mu\text{g/mL})$ was obtained; considering a system resolution of 78
53 pm, a limit of detection of 30 ng/mL can be extrapolated, which indicates a moderate
54
55
56
57
58
59
60

1
2
3 sensitivity. Nevertheless, measurements with microdisks lacking the horizontal slot would allow
4 extracting the contribution of the slot region in the sensitivity.
5
6

7
8 Recently Di Falco have combined slotted waveguides with a planar photonic crystal platform
9 [170], resulting in cavities with extremely high sensitivity as compared with conventional
10 waveguide photonic crystals, reaching Q factors up to 50000 in air (4000 in liquid), a sensitivity
11 of 1500 nm/RIU, and a detection limit around $7 \cdot 10^{-6}$ RIU, quite remarkable for photonic
12 crystals, as discussed in the section above [171]. Unfortunately, no biosensing experiments with
13 these structures have been performed yet.
14
15
16
17

18
19 Overall, for slot nanophotonic structures, where the enhancement of sensitivity comes precisely
20 from the slot area, a key aspect to address is the controlled and optimum biofunctionalization
21 only in the slot region. This becomes especially tricky since the dimensions of the slot, usually
22 around 100-200 nm, can hinder the complete filling of the area when sample and solutions are
23 delivered. It is of paramount importance to design optimal micro or nanofluidics, which, in
24 combination with proper surface modification, ensures a complete and uniform delivery of the
25 solution and an appropriate wettability of the surface. Until solving the current technical
26 limitations, slot waveguide sensors will not be able to show the exceptional performances for
27 biosensing theoretically predicted.
28
29
30
31
32
33

34
35 An original type of integrated photonic structures has recently been developed by Holgado *et*
36 *al.*, with significant novelties in terms of read-out interrogation at micron and sub-micron
37 sensing spot size. The group has designed a lattice of submicron photonic nanostructures of
38 SiO_2/Si or polymer pillars whose fabrication is compatible with standard semiconductor
39 technology at wafer level (see figure 7.D). Discrete photonic cells based on (i) cone-shaped
40 holes of 650 nm top diameter and 396 bottom diameter and lattice parameter of 800 nm [172]
41 and (ii) SU-8 nanopillars of 499 nm height, 136 nm width and 750 nm lattice pitch [173] have
42 been fabricated. An optical vertical interrogation at the single nanostructure level has been
43 implemented based on three independent reflectivity measurements (as a function of wavelength
44 by spectrometry, as a function of incidence angle by reflectometry, and as a function of phase
45 shift by ellipsometry) [172,174]. Reflectivity measurements are very sensitive to any change of
46 the refractive index in close contact to the pillars which can be used for the development of
47 highly sensitive biosensors after an appropriate biofunctionalization.
48
49
50
51
52
53
54
55
56

57
58 This novel label-free biosensing scheme has several advantages, besides those derived from the
59 microelectronics-based fabrication: (i) the use of three different readout techniques improves the
60 reproducibility and the reliability of the measurements; (ii) depending on the dimensions of the

1
2
3 nanostructures and the separation among them, the evanescent field can be strongly confined in
4 those areas, increasing the surface sensitivity towards biomolecule interactions; (iii) as the
5 optical sensing is based on the use of a tightly vertically focused beam, light coupling is
6 avoided, which simplifies the analyses and enables evaluation at spots of 0.9 μm . As the
7 dimensions of individual structures are submicron-sized, it is possible to analyze single
8 structures. Overall, all these aspects are very attractive for future commercialization of
9 integrated and disposable chips with high throughput capabilities.

10
11
12
13
14
15
16 Besides the characterization of the structure using solutions with different refractive indexes
17 [172], preliminary biosensing experiments have recently been performed by covalent
18 immobilization of BSA onto the nanopillars and the subsequent biodetection of the interaction
19 with the specific antibody, reaching sensitivities around 3 ng/mL [175] under static conditions.
20 Further implementation of an appropriate microfluidic flow cell and a flow delivery system will
21 allow the optimum infiltration of the solutions through the whole sensor lattice. This will be the
22 next step for these promising devices that could offer multiplexing evaluation of at least 1200
23 samples per hour.

31 **3.6. Optonanomechanical sensors**

32 Optomechanical (OM) sensing is a novel technology derived from the standard micro and nano-
33 electromechanical systems widely employed during the last years in the biosensing field.
34 Specifically, nanomechanical systems based on silicon microcantilevers have demonstrated an
35 extremely high sensitivity in the measurement of frequency [176,177] and deflection changes
36 [178] due to mass accumulation or biosensing interactions [179-183], and in the measurement
37 of forces between single molecules [184] or even of forces arising from single electron spin
38 [185].

39
40
41
42
43 However, in order to achieve full working prototypes as lab-on-a-chip biosensors, the
44 commonly used optical readout method for nanomechanical sensors have severe limitations
45 related to the complex optical alignment of multiple cantilevers at the same time, and the
46 diffraction constraints when the size of the cantilever is reduced below the wavelength. In an
47 optonanomechanical sensor, the cantilever itself is an optical waveguide which output intensity
48 is a function of the bending induced by a biomolecular interaction. With this new configuration
49 is possible to overcome the aforementioned limitations of standard nanomechanical sensors.
50 This microscale optical waveguide cantilevers are mainly addressed to sensing applications and
51 several works have demonstrated its motion sensitivity. The working principle of the optical
52 microcantilevers do not rely on refractive index changes, but on the microcantilever bending or
53 resonance frequency shift, measured through the light intensity collected at the cantilever free
54 end. The limit of detection can be evaluated in terms of analyte concentration (i.e. in ng/mL or
55
56
57
58
59
60

1
2
3 molarity), according to the cantilever bending (in nm) or frequency change (Hz), or according to
4 surface mass density (pg/mm^2).
5
6
7

8 The most extended configuration for biosensing is the end-coupled which consists of a
9 microcantilever acting as a waveguide; the light propagates along the cantilever until reaching
10 the free end. After crossing a small gap, light is collected by an output waveguide (see Figure
11 8.A). Several parameters can have an influence on the system sensitivity, such as the distance
12 from the cantilever edge to the collecting waveguide, the coupling efficiency or the cantilever
13 material and rigidity. Different materials, cantilever shapes, and light coupling methods have
14 been investigated. The device fabricated by Zinoviev *et al.* employs an array of 20 waveguide
15 silicon dioxide microcantilevers, each one of them connected with a silicon nitride multimode
16 input and output waveguide; the light from the input waveguide is coupled to the cantilever
17 through the overlapping of the evanescent field [186] (Figure 8.B). With this configuration, the
18 cantilever displacement can be detected with a resolution of $18 \text{ fm Hz}^{-1/2}$, sensitivity comparable
19 to the standard optical lever method, which indicates its suitability for biosensing applications.
20
21
22
23
24
25
26
27
28

29 A silicon microcantilever etched to form a single mode waveguide rib, with a capture
30 asymmetrical multimode waveguide that terminates in a Y-branch, was proposed by Noh *et al.*
31 [187]. The Y-branch forms a differential signal that is monotonically dependent on the
32 microcantilever deflection, achieving a signal sensitivity of $1.4 \times 10^{-4} \text{ nm}^{-1}$. More recently, the
33 same group has reported a sensitivity enhancement by modifying the mode structure of double-
34 step rib waveguides used to capture light, reaching a sensitivity comparable to the optical lever
35 method [188]. Besides the use of silicon material, there is an increasing interest on polymeric
36 materials for waveguides fabrication. Employing SU-8 [189-192] and PDMS [193] polymers
37 several groups have already developed integrated optical waveguide cantilevers. Indium
38 phosphide has also been employed showing up as a suitable material for the fabrication of
39 electrostatically actuated end-coupled optical waveguide MEMs [194]. Other works suggest the
40 use of silicon photonic crystals for guiding the light through the microcantilever [195-197], or
41 on chip in-plane Fabry-Pérot interferometer readout [198]. Working with arrays of optical
42 waveguide microcantilevers is more challenging as a multiplexed input of the light in each
43 cantilever must be achieved. With this aim, different strategies have been proposed, such as
44 using diffraction gratings [199], a network of waveguide splitters [200] or integrated silicon
45 light sources and detectors self-aligned to silicon waveguides [201]. A higher integration and
46 scale reduction of these nanophotonic platforms allow the direct actuation of MEMs by the
47 force exerted by the propagated photons. Li *et al.* suggested two different integrated photonic
48 platforms designs [202,203]: an embedded beam resonator with an on-chip interferometer for
49 the displacement sensing, and a pair end-to-end coupled waveguide cantilevers. Both platforms
50
51
52
53
54
55
56
57
58
59
60

1
2
3 include two input/output grating couplers at the end of the waveguides for light coupling. A
4 displacement sensitivity of $40 \text{ fm Hz}^{-1/2}$ was achieved with the end-to-end coupled cantilevers
5 working under vacuum conditions.
6
7

8
9
10 However, to our knowledge, the application of this technology to the biosensor field is scarce.
11 For example, Koev *et al.* were able to detect homocysteine in liquid at a lowest concentration of
12 $10 \text{ }\mu\text{M}$ with a minimum detectable cantilever bending of 5 nm [191]. Nordin's group has
13 recently demonstrated the integration of a 16 microcantilever array using in-plane photonic
14 readout with a 2-layer PDMS-based microfluidic chip which integrated valves to control the
15 fluid flow through the microchannels. However, only the study of the transient response of the
16 microcantilevers was reported. [204] A higher integration and scale reduction of these mechano-
17 photonic platforms can be easily achieved, producing devices with a very small mass and low
18 dissipation, ideal for fundamental studies [205-208], although with no biological applications
19 reported so far.
20
21
22
23
24
25

26 27 28 **4. Current commercial technologies based on label-free photonic biosensors**

29 Some of the technologies described in the previous sections have evolved into commercial
30 platforms for label-free detection, which has exponentially expanded the number and variety of
31 applications in biotechnology, biology, and clinical analysis. In this section we will give an
32 overview of the most relevant biosensor devices based on integrated optical transducers that
33 have been successfully transferred into the market. As it can be appreciated, none of them has
34 achieved the status of complete "lab-on-a-chip" portable platform with compact and reduced
35 size. Instead, most of them are bulky instruments mainly for laboratory use with a complex and
36 challenging road to achieve point-of-care status. However, all of them have demonstrated the
37 excellent performances of the integrated optics-based sensors in terms of sensitivity and
38 automation, and, in some cases, even in terms of multiplexing (allowing medium to high
39 throughput analysis).
40
41
42
43
44
45
46
47
48

49 **Farfield**

50 In 2000 Farfield Group launched into the market the AnaLight® interferometer based on Dual
51 Polarization Interferometry (DPI). Whereas all the interferometric schemes previously discussed
52 employ only one polarization, DPI uses both TM and TE polarizations in a sensing transducer
53 that mimics Young configuration. By simultaneously measuring both polarizations,
54 determination of the thickness and the refractive index of a film adsorbed on the sensor surface
55 can be done under real time conditions, which increases the versatility of the device for
56 advanced and complex measurements. Sensitivity of the instrument reaches refractive index
57 variation of 10^{-7} RIU, and a mass surface sensitivity of 0.1 pg/mm^2 . Two simultaneous
58
59
60

1
2
3 evaluations are possible by a dual-channel flow cell with small sample-volume capability (<50
4 μL). A bulkier platform, AnaLight® 4D Workstation (Analysis Station: 90x48x35 cm and
5 Pump Size 28x23x16 cm) is also commercialized for automatic sampling using vials, and 96
6 and 384 wells format. The instrument has been exploited for diverse biosensing evaluations,
7 using surfaces already preactivated and functionalized with appropriate chemistry. Among
8 others, the platform allows for thermodynamics, kinetics and affinity studies, such as protein
9 interaction studies, protein conformational changes, specific biodetection and biomolecular
10 interactions, surface density evaluation, lipid bilayer formation and characterization,
11 biocompatibility studies and protein or lipid aggregation analyses. The main disadvantage is the
12 limitation to only two samples due to the microfluidics system and the read-out electronics.
13
14
15
16
17
18
19
20

21 **SRU Biosystems**

22 SRU Biosystems, Inc. has developed the BIND™ Biosensor, based on the use of photonic
23 crystals in a grating configuration. The platform offers high multiplexed capabilities in a
24 microplate format (up to 1536 wells). The instrument has a high level of resolution (in the pm
25 level) and a broad dynamic range, which ensures the analysis of both small molecules and large
26 entities as cells or bacteria. The sensing surfaces are modified following optimized protocols to
27 enable both cell-based and biochemical assays with excellent performance. Different readers are
28 available both for single point mode and imaging mode. The instrument has fast detection times
29 (96-well in 30 seconds, 384-well in 1 minute, 1536-well in 3 minutes), or even faster with an
30 advanced readout mode (96-well in 8 seconds, 384-well in 15 seconds, 1536-well in 45
31 seconds). Among others, the platform has demonstrated its usefulness in diverse applications as
32 for cell morphology and adhesion assays, ion channel assays, small molecule and fragment
33 screening, and for the analysis of interactions of large genomic, protein, peptide or antibody
34 libraries against a wide range of biochemical targets.
35
36
37
38
39
40
41
42
43
44

45 **Corning**

46 A quite similar technology to BIND™ Biosensor has been marketed by Corning. Epic® System
47 is a high throughput screening platform based on waveguide resonant gratings. This device
48 reaches a detection limit around 5 pg/mm^2 and has a broad dynamic range. Some functionalized
49 surfaces are available (three types: cell-based, biochemical or fibronectin-coated, also for cell
50 assays). The instrument can be coupled to an automatic liquid handler in order to enhance its
51 throughput performance and has a rate analysis of 6 s/microplate requiring sample volumes of
52 15-80 μL . A main disadvantage is related to the dimensions of the whole instrumentation
53 (0.83m x 1.15 m x 1.98 m) and its high price, which can limit its implementation in laboratories
54 and other institutions. A benchtop version of the reader (EnSpire® Multimode Plate Reader, in
55 collaboration with Perkin-Elmer) is also currently commercialized, with more convenient
56
57
58
59
60

1
2
3 features, which allows for label-free as well as for fluorescence, absorbance and luminescence
4 detection.
5
6

8 **Axela**

9
10 Axela group has launched the dotLab® System, an instrument based on diffractive optical
11 gratings. The grating is fabricated on the lower area of a prism-shaped surface, which is
12 integrated in a 10 µL flow channel disposable plastic chip. Each dot lab sensor contains eight
13 assay spots aligned with the linear flow channel for multiple assays. The fluidic controller can
14 work under static, continuous flow or constant mixing mode. The samples and solutions are
15 delivered to the sensor by an automated sampling system (from reagent bottles or 96-well
16 microplates), allowing real time evaluation. The dotLab® is provided with several attachment
17 chemistries (i.e. streptavidin modified, Protein G, Goat-Anti-Mouse-Fc or for covalent binding)
18 which increases the flexibility for the coupling of bioreceptors to the surface. Features of the
19 device include label-free and quantitative evaluation within a broad dynamic range. The
20 dimensions are comparatively smaller than for SRU and Corning instruments (43.5 cm H x 57,9
21 cm W x 69.3 cm D) but the multiplexed capabilities are more limited, since the analysis time is
22 slower and only eight simultaneous tests are possible. The instrument can be used for protein-
23 protein interaction studies, epitope mapping, or for the detection and quantification of proteins,
24 among others.
25
26
27
28
29
30
31
32
33
34

35 **Microvacuum**

36
37 Microvacuum Ltd. manufactures the OWLS System based on Optical Waveguide Lightmode
38 Spectroscopy [63]. In this sensor, polarized light is coupled by an input grating and guided by
39 total internal reflection to the end of the waveguide where is detected by the photodiodes. The
40 light mode spectrum can be obtained by varying the angle of incidence, whereas the flow cell is
41 fixed over the grating coupler waveguide sensor chip. From the mode spectra it is possible to
42 determine the physical parameters of the cover medium (thickness, refractive index, density
43 etc.). The chip is mounted on a precision goniometer which provides the adjustment of the angle
44 of incidence. It operates under continuous flow rate for real time evaluation. The instrument has
45 a compact small-to-medium size and includes the optomechanical system, the electronics,
46 temperature control and the sensor holder, together with the injection unit (with several volume
47 sample loops), although the fluidic pump is external. The data acquisition and the software
48 evaluate the refractive index and thickness of the adsorbed layer, and provide qualitative
49 kinetics information. The instrument can be applied for biomolecular interaction studies
50 (protein-protein, nucleic acids, membrane protein-lipid bilayer...), cell-based assays, surface
51 coverage characterization, drug screening or kinetic analysis. The sensor surface has general
52 features which can be modified on request to improve performance (i.e. dimensions of the chip,
53
54
55
56
57
58
59
60

1
2
3 dielectric coatings of the surface, passivation or functionalization with silanes). The instrument
4 can be combined with two additional units: an electro-chemical system and a fluorescent
5 measuring system. Unfortunately, the instrument has very limited throughput capabilities since
6 it can only perform single measurements on relatively large chips (around 12 mm x 8 mm).
7
8
9

10 11 **Genalyte**

12 Relatively new, Genalyte has started commercializing the Maverick Detection System based on
13 an array of microring resonator silicon sensors. The instrument currently in the market is the
14 third generation and has a compact design, which delivers the samples (typically less than 25
15 μL) from a 96-well plate into the plastic chip consumable which contains the sensing surface,
16 consisting of an array of silicon microrings (from 1 up to 128 in each surface, including 8
17 controls). The system can perform simultaneous measurements in real time, and results are
18 available in a time scale between 5-45 min, depending on the concentration to be detected.
19 Some of the features of the instrument are the possibility to perform kinetics measurements
20 (using 2 flow channels which delivery samples to 16 sensors each one) or end-point
21 measurements using 96-well footprint; it has a wide dynamic range up to eight orders of
22 magnitude, with sensitivities close to 0.1 ng/mL, a limit of detection around 0.1 fg and it is able
23 to measure targets of molecular weight of only 10 Da.
24
25
26
27
28
29
30
31
32
33

34 **5. Integration in lab-on-a-chip platforms**

35 The major challenge in the silicon photonic biosensor field is to achieve fully operative lab-on-
36 a-chip platform with on-chip detection. Further efforts are addressed to keep high level of
37 sensitivities and to develop complete Si CMOS compatible integrated devices that incorporate
38 the photonic systems with microfluidics and the optoelectronics [46,209,210]. For the
39 development of a complete photonic lab-on-a-chip device, several units must be incorporated on
40 the same platform: (i) the photonic sensors, (ii) the flow cells and the flow delivery system,
41 including miniaturized valves and pumps (iii) the light sources and photodetectors array or
42 miniaturized CCD cameras (iv) processing electronics (i.e. CMOS) and, (v) final packaging
43 with the required firmware and software (see Figure 9). Integration could be monolithic (all
44 functionalities are incorporated in one single chip) or hybrid (functionalities are separated on
45 several chips). In the monolithic approach photodiodes and lasers can be embedded in the
46 waveguides. Due to economic and technical reasons the hybrid approach is mostly preferred,
47 where the components are settled apart. Even if the individual components are well-known, the
48 subsystem interfaces between them are difficult to optimize and these are still the major barriers
49 to be surpassed. With the hybrid arrangement, the optoelectronics and the read-out system can
50 be reusable and only the cartridge containing the sensing chip with the microfluidics for
51 independent applications can be interchanged.
52
53
54
55
56
57
58
59
60

1
2
3
4
5 Most of the work done so far mainly includes the integration of the sensors and the fluidics
6 (which has emerged as a new discipline called “optofluidics”) and the development of discrete
7 components for future integration [211] Few examples can be found in the literature of complete
8 lab-on-a-chip developments. For instance Jokerst *et al.* have developed an integrated
9 evanescent-field multimode Mach-Zehnder interferometric sensor fully compatible with Si-
10 CMOS process [212] with a LOD of 2.5×10^{-6} RIU. In further refinements a fully integrated
11 version was in place with interferometric sensors of only 5 mm length which reached a
12
13 refractive index sensitivity of $\sim 9.2 \times 10^{-7}$ RIU [212]. Unfortunately, this device has not been
14
15
16
17
18
19
20
21
22
23
24 tested yet for biosensing applications.
25
26

27 A monolithically integrated interferometric lab-on-a-chip biosensor is under development
28 within the frame of an European project [213]. The principle of operation of the PYTHIA lab-
29 on-a-chip is based on broad-Band Mach-Zehnder interferometer sensors and including lasers,
30 photodetectors and microfluidics. Femtosecond laser micromachining is nowadays an emerging
31 tool for the fabrication of monolithic optofluidic devices, allowing the direct fabrication of
32 integrated optical devices and microfluidics in fused silica chips. [32,214]
33
34
35
36
37

38 Lab-on-a-chip with the on-chip detection is still very much a work in progress, but last advances
39 in integrated optics-based biosensors and optofluidics indicate that they could eventually be
40 achieved in the near-medium future. Cutting edge technological progress will give raise to a
41 robust product that could run on an automated system minimizing operator skills.
42
43
44
45

46 6- Future outlook

47 During last years a myriad of different developments at the biosensor field using many diverse
48 technologies and devices has been appearing, such as nanomechanical or MEMS resonators
49 sensors, semiconductor wires-based transducers, highly integrated microelectrodes, carbon
50 nanotubes-based sensors, localized surface plasmon resonance or SERS in metal nanostructures,
51 but none of them has shown the excellent performances for label-free sensing achieved by
52 photonic and nanophotonic devices based on integrated optics, as can be deduced from their
53 excellent limits of detection in real biosensing (shown along this review). Some commercial
54 optical biosensors have been introduced into the market but most of them are bulky and
55 expensive and only offer a general technology, with a limited number of dedicated applications.
56
57
58
59
60

1
2
3
4
5 Integrated optics technology is opening the way towards truly portable lab-on-a-chip platforms
6 which could be employed outside the laboratory. But still limitations in the technology,
7 problems in the integration of all the components in one single microsystem and the connection
8 with real world applications should be surpass. In the near future, we will employ lab-on-a-chip
9 biosensor devices for assessing the safety of our food or beverages, for fast environmental
10 pollution identification and for the fast identification of illness at urgency or by diagnostics
11 people at the doctor office in a more comfortable way than it is done today. Due to the intensive
12 research effort which is being done at public institutions and at small, medium and large private
13 companies there are no doubts that lab-on-chip hand-held devices will be a reality in our future
14 society and will impact very positively our lifestyle.
15
16
17
18
19
20
21

22 **Acknowledgements**

23 Authors acknowledge the financial support from Fundación M. Botín and SENA project (TSI-
24 020301-2008-11) from the Spanish Ministry of Industry. M.A. acknowledges financial support
25 from Juan de la Cierva Program (MICINN-JDC) from the Spanish Ministry of Science and
26 Innovation.
27
28
29
30
31
32
33
34
35
36
37
38
39
40
41
42
43
44
45
46
47
48
49
50
51
52
53
54
55
56
57
58
59
60

References

- [1] L. M. Lechuga, in *Biosensors and Modern Biospecific Analytical Techniques*, edited by L. Gorton (Elsevier Science BV, Amsterdam, Netherlands, 2005), Vol. XLIV.
- [2] J. V. Jokerst, J. W. Jacobson, B. D. Bhagwandin, P. N. Floriano, N. Christodoulides, and J. T. McDevitt, *Anal. Chem.* **82** (5), 1571 (2010).
- [3] F. S. Ligler, *Anal. Chem.* **81** (2), 519 (2008).
- [4] J. Homola, *Chem. Rev.* **108** (2), 462 (2008).
- [5] E. Mauriz, A. Calle, J. J. Manclus, A. Montoya, A. Hildebrandt, D. Barcelo, and L. M. Lechuga, *Biosens. Bioelectron.* **22** (7), 1410 (2007).
- [6] J. Treviño, A. Calle, J. M. Rodríguez-Frade, M. Mellado, and L. M. Lechuga, *Clin. Chim. Acta* **403** (1-2), 56 (2009).
- [7] L. Carrascosa, A. Calle, and L. Lechuga, *Anal. Bioanal. Chem.* **393** (4), 1173 (2009).
- [8] D. Erickson, S. Mandal, A. Yang, and B. Cordovez, *Microfluid. Nanofluid.* **4** (1), 33 (2008).
- [9] A. L. Washburn and R. C. Bailey, *Analyst* **136** (2), 227 (2011).
- [10] F. Vollmer and S. Arnold, *Nat. Meth.* **5** (7), 591 (2008).
- [11] X. D. Fan, I. M. White, S. I. Shopova, H. Zhu, J. D. Suter, and Y. Sun, *Anal. Chim. Acta* **620**, 8 (2008).
- [12] P. Lambeck, V., *Meas. Sci. Technol.* **17** (8), R93 (2006).
- [13] C. Monat, P. Domachuk, and B. J. Eggleton, *Nat. Photonics* **1** (2), 106 (2007).
- [14] L. S. Wong, F. Khan, and J. Micklefield, *Chem. Rev.* **109** (9), 4025 (2009).
- [15] B. Prieto-Simon, M. Campas, and J. L. Marty, *Protein Pept. Lett.* **15** (8), 757 (2008).
- [16] F. Rusmini, Z. Zhong, and J. Feijen, *Biomacromolecules* **8** (6), 1775 (2007).
- [17] J. Diao, D. Ren, J. R. Engstrom, and K. H. Lee, *Anal. Biochem.* **343** (2), 322 (2005).
- [18] A. Arafat, M. Giesbers, M. Rosso, E. J. R. Sudhölter, K. Schroën, R. G. White, L. Yang, M. R. Linford, and H. Zuilhof, *Langmuir* **23** (11), 6233 (2007).
- [19] A. Arafat, K. Schroën, L. C. P. M. de Smet, E. J. R. Sudhölter, and H. Zuilhof, *J. Am. Chem. Soc.* **126** (28), 8600 (2004).
- [20] M.-J. Bañuls, V. González-Pedro, C. A. Barrios, R. Puchades, and Á. Maquieira, *Biosens. Bioelectron.* **25** (6), 1460 (2010).
- [21] P. Wu, P. Högbe, and D. W. Grainger, *Biosens. Bioelectron.* **21** (7), 1252 (2006).
- [22] A. Akkoyun and U. Bilitewski, *Biosens. Bioelectron.* **17** (8), 655 (2002).
- [23] S. Sharma, R. W. Johnson, and T. A. Desai, *Biosens. Bioelectron.* **20** (2), 227 (2004).
- [24] M. Cerruti, S. Fissolo, C. Carraro, C. Ricciardi, A. Majumdar, and R. Maboudian, *Langmuir* **24** (19), 10646 (2008).

- 1
2
3 [25] N.-P. Huang, R. Michel, J. Voros, M. Textor, R. Hofer, A. Rossi, D. L. Elbert, J. A.
4 Hubbell, and N. D. Spencer, *Langmuir* **17** (2), 489 (2001).
5
6 [26] N.-P. Huang, J. Vörös, S. M. De Paul, M. Textor, and N. D. Spencer, *Langmuir* **18** (1),
7 220 (2002).
8
9 [27] M. P. Schwartz, F. Cunin, R. W. Cheung, and M. J. Sailor, *Phys. Status Solidi A* **202**
10 (8), 1380 (2005).
11
12 [28] R. Marie, A. B. Dahlin, J. O. Tegenfeldt, and F. Hook, *Biointerphases* **2** (1), 49 (2007).
13
14 [29] B. Drapp, J. Piehler, A. Brecht, G. Gauglitz, B. J. Luff, J. S. Wilkinson, and J.
15 Ingenhoff, *Sens. Actuators B* **39** (1-3), 277 (1997).
16
17 [30] B. J. Luff, J. S. Wilkinson, J. Piehler, U. Hollenbach, J. Ingenhoff, and N. Fabricius, J.
18 *Lightwave Technol.* **16** (4), 583 (1998).
19
20 [31] Z.-m. Qi, N. Matsuda, K. Itoh, M. Murabayashi, and C. R. Lavers, *Sens. Actuators B* **81**
21 (2-3), 254 (2002).
22
23 [32] A. Crespi, Y. Gu, B. Ngamsom, H. J. W. M. Hoekstra, C. Dongre, M. Pollnau, R.
24 Ramponi, H. H. van den Vlekkert, P. Watts, G. Cerullo, and R. Osellame, *Lab Chip* **10**
25 (9), 1167 (2010).
26
27 [33] A. Dér, S. Valkai, A. Mathesz, I. Andó, E. K. Wolff, and P. Ormos, *Sens. Actuators B*
28 **151** (1), 26 (2010).
29
30 [34] B. Y. Shew, C. H. Kuo, Y. C. Huang, and Y. H. Tsai, *Sens. Actuators A* **120** (2), 383
31 (2005).
32
33 [35] B. Y. Shew, Y. C. Cheng, and Y. H. Tsai, *Sens. Actuators A* **141** (2), 299 (2008).
34
35 [36] L. M. Lechuga, A. T. M. Lenferink, R. P. H. Kooyman, and J. Greve, *Sens. Actuators B*
36 **25** (1-3), 762 (1995).
37
38 [37] E. F. Schipper, A. M. Brugman, C. Dominguez, L. M. Lechuga, R. P. H. Kooyman, and
39 J. Greve, *Sens. Actuators B* **40** (2-3), 147 (1997).
40
41 [38] R. G. Heideman and P. V. Lambeck, *Sens. Actuators B* **61** (1-3), 100 (1999).
42
43 [39] F. Brosinger, H. Freimuth, M. Lacher, W. Ehrfeld, E. Gedig, A. Katerkamp, F. Spener,
44 and K. Cammann, *Sens. Actuators B* **44** (1-3), 350 (1997).
45
46 [40] M. Weisser, G. Tovar, S. Mittler-Neher, W. Knoll, F. Brosinger, H. Freimuth, M.
47 Lacher, and W. Ehrfeld, *Biosens. Bioelectron.* **14** (4), 405 (1999).
48
49 [41] F. Prieto, B. Sepulveda, A. Calle, A. Llobera, C. Dominguez, A. Abad, A. Montoya,
50 and L. M. Lechuga, *Nanotechnology* **14** (8), 907 (2003).
51
52 [42] F. Prieto, A. Llobera, D. Jimenez, C. Domenguez, A. Calle, and L. M. Lechuga, J.
53 *Lightwave Technol.* **18** (7), 966 (2000).
54
55 [43] F. Prieto, L. M. Lechuga, A. Calle, A. Llobera, and C. Dominguez, *J. Lightwave*
56 *Technol.* **19** (1), 75 (2001).
57
58
59
60

- 1
2
3 [44] K. Zinoviev, Laura G. Carrascosa, Jose Sanchez del Rio, Borja Sepulveda, Carlos
4 Dominguez, and L. M. Lechuga, *Adv. Opt. Tech.* **2008** (Article ID: 383927), 6 p
5 (2008).
6
7
8 [45] F. Prieto, B. Sepúlveda, A. Calle, A. Llobera, C. Domínguez, and L. M. Lechuga, *Sens.*
9 *Actuators B* **92** (1-2), 151 (2003).
10
11 [46] L. M. Lechuga, E. Mauriz, B. Sepúlveda, J. Sánchez del Río, A. Calle, G. Armelles, and
12 C. Dominguez, in *Proceedings of the NATO Advanced Research Workshop on*
13 *Frontiers in Planar Lightwave Circuit Technology*, edited by Janz S., J. Ctyroki, and s.
14 Tanev (Kluwer, Ottawa, Canada, 2006), Vol. 216, pp. 287.
15
16 [47] A. Brandenburg, R. Krauter, C. Künzel, M. Stefan, and H. Schulte, *Appl. Opt.* **39** (34),
17 6396 (2000).
18
19 [48] K. Schmitt, B. Schirmer, C. Hoffmann, A. Brandenburg, and P. Meyrueis, *Biosens.*
20 *Bioelectron.* **22** (11), 2591 (2007).
21
22 [49] E. Brynda, M. Houska, A. Brandenburg, and A. Wikerstål, *Biosens. Bioelectron.* **17** (8),
23 665 (2002).
24
25 [50] C. Hoffmann, K. Schmitt, A. Brandenburg, and S. Hartmann, *Anal. Bioanal. Chem.* **387**
26 (5), 1921 (2007).
27
28 [51] T. Nagel, E. Ehrentreich-Förster, M. Singh, K. Schmitt, A. Brandenburg, A. Berka, and
29 F. F. Bier, *Sens. Actuators B* **129** (2), 934 (2008).
30
31 [52] D. Hradetzky, C. Mueller, and H. Reinecke, *J. Opt. A: Pure Appl. Opt.* **8** (7), S360
32 (2006).
33
34 [53] A. Ymeti, J. S. Kanger, J. Greve, P. V. Lambeck, R. Wijn, and R. G. Heideman, *Appl.*
35 *Opt.* **42** (28), 5649 (2003).
36
37 [54] A. Ymeti, J. Greve, P. V. Lambeck, R. Wijn, R. G. Heideman, and J. S. Kanger, *Appl.*
38 *Opt.* **44** (17), 3409 (2005).
39
40 [55] A. Ymeti, J. S. Kanger, J. Greve, G. A. J. Besselink, P. V. Lambeck, R. Wijn, and R. G.
41 Heideman, *Biosens. Bioelectron.* **20** (7), 1417 (2005).
42
43 [56] A. Ymeti, J. Greve, P. V. Lambeck, T. Wink, S. W. F. M. van Hovell, T. A. M.
44 Beumer, R. R. Wijn, R. G. Heideman, V. Subramaniam, and J. S. Kanger, *Nano. Lett.* **7**
45 (2), 394 (2007).
46
47 [57] B. H. Schneider, J. G. Edwards, and N. F. Hartman, *Clin. Chem.* **43** (9), 1757 (1997).
48
49 [58] B. H. Schneider, E. L. Dickinson, M. D. Vach, J. V. Hoijer, and L. V. Howard, *Biosens.*
50 *Bioelectron.* **15** (1-2), 13 (2000).
51
52 [59] B. H. Schneider, E. L. Dickinson, M. D. Vach, J. V. Hoijer, and L. V. Howard, *Biosens.*
53 *Bioelectron.* **15** (11-12), 597 (2000).
54
55 [60] J. Xu, D. Suarez, and D. Gottfried, *Anal. Bioanal. Chem.* **389** (4), 1193 (2007).
56
57
58
59
60

- 1
2
3 [61] K. E. Zinoviev, A. B. González-Guerrero, C. Domínguez, and L. M. Lechuga, J.
4 Lightwave Technol. **29** (13), 1926 (2011).
5
6 [62] K. Erdélyi, A. G. Frutos, J. J. Ramsden, I. Szendro, and G. Voirin, *Grating-Based*
7 *Optical Biosensors*. (John Wiley & Sons, Ltd, 2008).
8
9 [63] J. Vörös, J. J. Ramsden, G. Csúcs, Szendro, I., S. M. De Paul, M. Textor, and N. D.
10 Spencer, Biomaterials **23** (17), 3699 (2002).
11
12 [64] P. M. Nellen, K. Tiefenthaler, and W. Lukosz, Sens. Actuators **15** (3), 285 (1988).
13
14 [65] P. M. Nellen and W. Lukosz, Sens. Actuators B **1** (1-6), 592 (1990).
15
16 [66] W. Lukosz, D. Clerc, P. M. Nellen, C. Stamm, and P. Weiss, Biosens. Bioelectron. **6**
17 (3), 227 (1991).
18
19 [67] W. Lukosz, P. M. Nellen, C. Stamm, and P. Weiss, Sens. Actuators B **1** (1-6), 585
20 (1990).
21
22 [68] F. F. Bier, R. Jockers, and R. D. Schmid, Analyst **119** (3), 437 (1994).
23
24 [69] F. F. Bier and R. D. Schmid, Biosens. Bioelectron. **9** (2), 125 (1994).
25
26 [70] R. Polzius, F. F. Bier, U. Bilitewski, V. Jäger, and R. D. Schmid, Biotechnol. Bioeng.
27 **42** (11), 1287 (1993).
28
29 [71] R. Polzius, T. Schneider, F. F. Bier, U. Bilitewski, and W. Koschinski, Biosens.
30 Bioelectron. **11** (5), 503 (1996).
31
32 [72] R. Polzius, E. Diebel, F. F. Bier, and U. Bilitewski, Anal. Biochem. **248** (2), 269
33 (1997).
34
35 [73] A. Brandenburg, R. Polzius, F. Bier, U. Bilitewski, and E. Wagner, Sens. Actuators B
36 **30** (1), 55 (1996).
37
38 [74] J. Piehler, A. Brandenburg, A. Brecht, E. Wagner, and G. Gauglitz, Appl. Opt. **36** (25),
39 6554 (1997).
40
41 [75] F. F. Bier and F. W. Scheller, Biosens. Bioelectron. **11** (6-7), 669 (1996).
42
43 [76] F. F. Bier, F. Kleinjung, and F. W. Scheller, Sens. Actuators B **38** (1-3), 78 (1997).
44
45 [77] S. Grego, S. Naskar, A. M. Patel, A. Huffman, C. A. Bower, and B. R. Stoner, Proc.
46 SPIE **6123**, 61230D (2006).
47
48 [78] S. Grego, J. R. McDaniel, and B. R. Stoner, Sens. Actuators B **131** (2), 347 (2008).
49
50 [79] S. Grego, Y. Cao, C. A. Bower, B. R. Stoner, and T. J. Suleski, in *Integrated Optics:*
51 *Devices, Materials, and Technologies XI*, edited by Y. Sidorin and C. A. Waechter
52 (Spie-Int Soc Optical Engineering, Bellingham, 2007), Vol. 6475, pp. 47504.
53
54 [80] P. K. Yuen, N. H. Fontaine, M. A. Quesada, P. Mazumder, R. Bergman, and E. J.
55 Mozdy, Lab Chip **5** (9), 959 (2005).
56
57 [81] M. Wiki and R. E. Kunz, Opt. Lett. **25** (7), 463 (2000).
58
59 [82] K. Cottier, M. Wiki, G. Voirin, H. Gao, and R. E. Kunz, Sens. Actuators B **91** (1-3),
60 241 (2003).

- 1
2
3 [83] J. Adrian, S. Pasche, J. M. Diserens, F. Sanchez-Baeza, H. Gao, M. P. Marco, and G.
4 Voirin, *Biosens. Bioelectron.* **24** (11), 3340 (2009).
5
6 [84] J. Adrian, S. Pasche, D. G. Pinacho, H. Font, J. M. Diserens, F. Sanchez-Baeza, B.
7 Granier, G. Voirin, and M. P. Marco, *TrAC, Trends Anal. Chem.* **28** (6), 769 (2009).
8
9 [85] G. Suarez, Y. H. Jin, J. Auerswald, S. Berchtold, H. F. Knapp, J. M. Diserens, Y.
10 Leterrier, J. A. E. Manson, and G. Voirin, *Lab Chip* **9** (11), 1625 (2009).
11
12 [86] S. Pasche, M. Giazzon, B. Wenger, G. Franc, R. Ischer, G. J. Oostingh, and G. Voirin,
13 *Proced. Chem.* **1** (1), 738 (2009).
14
15 [87] J. Razumovitch, K. de Franca, F. Kehl, M. Wiki, W. Meier, and C. Vebert, *J. Phys.*
16 *Chem. B* **113** (24), 8383 (2009).
17
18 [88] R. W. Boyd and J. E. Heebner, *Appl. Opt.* **40** (31), 5742 (2001).
19
20 [89] S. Lee, S. C. Eom, J. S. Chang, C. Huh, G. Y. Sung, and J. H. Shin, *Opt. Express* **18**
21 (20), 20638 (2010).
22
23 [90] S. Lee, S. C. Eom, J. S. Chang, C. Huh, G. Y. Sung, and J. H. Shin, *Opt. Express* **18**
24 (11), 11209 (2010).
25
26 [91] A. Schweinsberg, S. Hocdé, N. N. Lepeshkin, R. W. Boyd, C. Chase, and J. E. Fajardo,
27 *Sens. Actuators B* **123** (2), 727 (2007).
28
29 [92] K. De Vos, I. Bartolozzi, E. Schacht, P. Bienstman, and R. Baets, *Opt. Express* **15** (12),
30 7610 (2007).
31
32 [93] K. M. De Vos, I. Bartolozzi, P. Bienstman, R. Baets, and E. Schacht, *XXX P Soc*
33 *Photo-Opt Ins* **6447**, K4470 (2007).
34
35 [94] X. Li, Z. Zhang, S. Qin, T. Wang, F. Liu, M. Qiu, and Y. Su, *Appl. Opt.* **48** (25), F90
36 (2009).
37
38 [95] T. Claes, J. G. Molera, K. De Vos, E. Schacht, R. Baets, and P. Bienstman, *IEEE*
39 *Photonics J.* **1** (3), 197 (2009).
40
41 [96] M. Iqbal, M. A. Gleeson, B. Spaugh, F. Tybor, W. G. Gunn, M. Hochberg, T. Baehr-
42 Jones, R. C. Bailey, and L. C. Gunn, *IEEE J. Sel. Top. Quant.* **16** (3), 654 (2010).
43
44 [97] M. S. Luchansky, A. L. Washburn, T. A. Martin, M. Iqbal, L. C. Gunn, and R. C.
45 Bailey, *Biosens. Bioelectron.* **26** (4), 1283 (2010).
46
47 [98] A. M. Armani, R. P. Kulkarni, S. E. Fraser, R. C. Flagan, and K. J. Vahala, *Science* **317**
48 (5839), 783 (2007).
49
50 [99] A. M. Armani, A. Srinivasan, and K. J. Vahala, *Nano. Lett.* **7** (6), 1823 (2007).
51
52 [100] A. M. Armani and K. J. Vahala, *Biophys. J.*, 29a (2007).
53
54 [101] H. K. Hunt, C. Soteropoulos, and A. M. Armani, *Sensors* **10** (10), 9317 (2010).
55
56 [102] X. M. Zhang, H. S. Choi, and A. M. Armani, *Appl. Phys. Lett.* **96** (15) (2010).
57
58
59
60

- 1
2
3 [103] A. Yalcin, K. C. Popat, J. C. Aldridge, T. A. Desai, J. Hryniewicz, N. Chbouki, B. E.
4 Little, K. Oliver, V. Van, C. Sai, D. Gill, M. Anthes-Washburn, M. S. Unlu, and B. B.
5 Goldberg, *IEEE J. Sel. Top. Quantum Electron.* **12** (1), 148 (2006).
6
7
8 [104] A. Ramachandran, S. Wang, J. Clarke, S. J. Ja, D. Goad, L. Wald, E. M. Flood, E.
9 Knobbe, J. V. Hryniewicz, S. T. Chu, D. Gill, W. Chen, O. King, and B. E. Little,
10 *Biosens. Bioelectron.* **23** (7), 939 (2008).
11
12 [105] A. Ksendzov and Y. Lin, *Opt. Lett.* **30** (24), 3344 (2005).
13
14 [106] P. Rabiei and W. H. Steier, presented at the Lasers and Electro-Optics Society, 2001.
15 LEOS 2001. The 14th Annual Meeting of the IEEE, 2001 (unpublished).
16
17 [107] M. Jazbinsek, P. Rabiei, C. Bosshard, and P. Gunter, *XXX Aip Conf Proc* **709**, 187
18 (2004).
19
20 [108] A. Chen, L. Dalton, T. Sherwood, A. K. Y. Jen, P. Rabiei, W. Steier, Y. Huang, G. T.
21 Paloczi, J. K. S. Poon, A. Scherer, and A. Yariv, *XXX P Soc Photo-Opt Ins* **5708**, 187
22 (2005).
23
24 [109] C.-Y. Chao and L. J. Guo, *Appl. Phys. Lett.* **83** (8), 1527 (2003).
25
26 [110] R. Dekker and et al., *J. Phys. D. Appl. Phys.* **40** (14), R249 (2007).
27
28 [111] K. De Vos, J. Girones, S. Popelka, E. Schacht, R. Baets, and P. Bienstman, *Biosens.*
29 *Bioelectron.* **24** (8), 2528 (2009).
30
31 [112] K. De Vos, J. Girones, T. Claes, Y. De Koninck, S. Popelka, E. Schacht, R. Baets, and
32 P. Bienstman, *IEEE Photonics J.* **1** (4), 225 (2009).
33
34 [113] J. Y. Byeon, F. T. Limpoco, and R. C. Bailey, *Langmuir* **26** (19), 15430 (2010).
35
36 [114] M. S. Luchansky and R. C. Bailey, *Anal. Chem.* **82** (5), 1975 (2010).
37
38 [115] A. L. Washburn, L. C. Gunn, and R. C. Bailey, *Anal. Chem.* **81** (22), 9499 (2009).
39
40 [116] A. L. Washburn, M. S. Luchansky, A. L. Bowman, and R. C. Bailey, *Anal. Chem.* **82**
41 (1), 69 (2010).
42
43 [117] A. J. Qavi and R. C. Bailey, *Angew. Chem. Int. Ed.* **49** (27), 4608 (2010).
44
45 [118] D. K. Armani, T. J. Kippenberg, S. M. Spillane, and K. J. Vahala, *Nature* **421** (6926),
46 925 (2003).
47
48 [119] A. M. Armani, D. K. Armani, B. Min, K. J. Vahala, and S. M. Spillane, *Appl. Phys.*
49 *Lett.* **87** (15) (2005).
50
51 [120] H. S. Choi, X. M. Zhang, and A. M. Armani, *Opt. Lett.* **35** (4), 459 (2010).
52
53 [121] R. V. Nair and R. Vijaya, *Prog. Quantum Electron.* **34** (3), 89 (2010).
54
55 [122] J. D. Joannopoulos, S. G. Johnson, J. N. Winn, and R. D. Meade, *Photonic Crystals.*
56 *Moding the Flow of Light.* (Princeton University Press, 2008).
57
58 [123] I. D. Block, N. Ganesh, M. Lu, and B. T. Cunningham, *IEEE Sens. J.* **8** (3-4), 274
59 (2008).
60
[124] B. Cunningham, P. Li, B. Lin, and J. Pepper, *Sens. Actuators B* **81** (2-3), 316 (2002).

- 1
2
3 [125] B. Cunningham, B. Lin, J. Qiu, P. Li, J. Pepper, and B. Hugh, *Sens. Actuators B* **85** (3),
4 219 (2002).
5
6 [126] B. Cunningham, J. Qiu, P. Li, and B. Lin, *Sens. Actuators B* **87** (2), 365 (2002).
7
8 [127] I. D. Block, L. L. Chan, and B. T. Cunningham, *Sens. Actuators B* **120** (1), 187 (2006).
9
10 [128] B. T. Cunningham, P. Li, S. Schulz, B. Lin, C. Baird, J. Gerstenmaier, C. Genick, F.
11 Wang, E. Fine, and L. Laing, *J. Biomol. Screening* **9** (6), 481 (2004).
12
13 [129] C. J. Choi and B. T. Cunningham, *Lab Chip* **6** (10), 1373 (2006).
14
15 [130] C. J. Choi and B. T. Cunningham, *Lab Chip* **7** (5), 550 (2007).
16
17 [131] C. J. Choi, I. D. Block, B. Bole, D. Dralle, and B. T. Cunningham, *IEEE Sens. J.* **9** (12),
18 1697 (2009).
19
20 [132] C. J. Choi, A. R. Belobraydich, L. L. Chan, P. C. Mathias, and B. T. Cunningham,
21 *Anal. Biochem.* **405** (1), 1 (2010).
22
23 [133] B. R. Schudel, C. J. Choi, B. T. Cunningham, and P. J. A. Kenis, *Lab Chip* **9** (12), 1676
24 (2009).
25
26 [134] B. T. Cunningham and L. Laing, *Expert Rev. Proteomics* **3** (3), 271 (2006).
27
28 [135] B. Lin, P. Li, and B. T. Cunningham, *Sens. Actuators B* **114** (2), 559 (2006).
29
30 [136] L. L. Chan, S. L. Gosangari, K. L. Watkin, and B. T. Cunningham, *Apoptosis* **12** (6),
31 1061 (2007).
32
33 [137] L. L. Chan, S. L. Gosangari, K. L. Watkin, and B. T. Cunningham, *Sens. Actuators B*
34 **132** (2), 418 (2008).
35
36 [138] M. F. Pineda, L. L. Y. Chan, T. Kuhlenschmidt, C. J. Choi, M. Kuhlenschmidt, and B.
37 T. Cunningham, *IEEE Sens. J.* **9** (4), 470 (2009).
38
39 [139] L. L. Chan, E. A. Lidstone, K. E. Finch, J. T. Heeres, P. J. Hergenrother, and B. T.
40 Cunningham, *Jala* **14** (6), 348 (2009).
41
42 [140] J. T. Heeres, S. H. Kim, B. J. Leslie, E. A. Lidstone, B. T. Cunningham, and P. J.
43 Hergenrother, *J. Am. Chem. Soc.* **131** (51), 18202 (2009).
44
45 [141] T. Xu, N. Zhu, M. Y. C. Xu, L. Wosinski, J. S. Aitchison, and H. E. Ruda, *Opt. Express*
46 **18** (6), 5420 (2010).
47
48 [142] D. F. Dorfner, T. Hurlimann, T. Zabel, L. H. Frandsen, G. Abstreiter, and J. J. Finley,
49 *Appl. Phys. Lett.* **93** (18), 181103 (2008).
50
51 [143] D. Dorfner, T. Zabel, T. Hurlimann, N. Hauke, L. Frandsen, U. Rant, G. Abstreiter, and
52 J. Finley, *Biosens. Bioelectron.* **24** (12), 3688 (2009).
53
54 [144] N. Skivesen, A. Tetu, M. Kristensen, J. Kjems, L. H. Frandsen, and P. I. Borel, *Opt.*
55 *Express* **15** (6), 3169 (2007).
56
57 [145] J. Garcia-Ruperez, V. Toccafondo, M. J. Banuls, J. G. Castello, A. Griol, S. Peransi-
58 Llopis, and A. Maquieira, *Opt. Express* **18** (23), 24276 (2010).
59
60

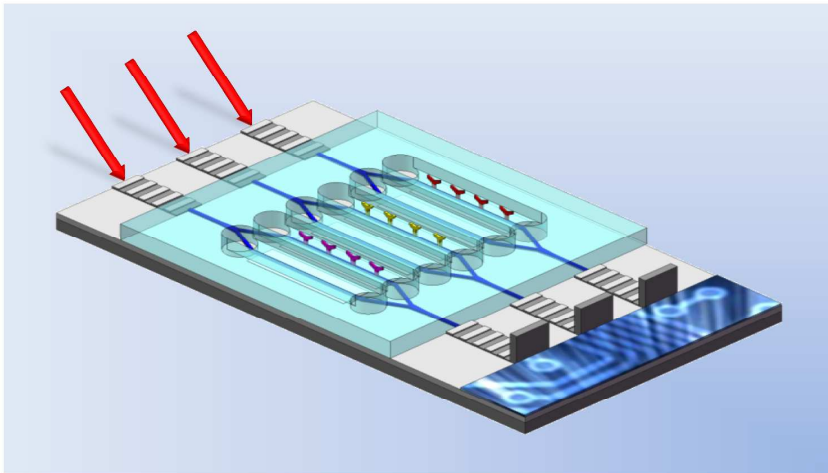
- 1
2
3 [146] V. Toccafondo, J. García-Rupérez, M. J. Bañuls, A. Griol, J. G. Castelló, S. Peransi-
4 Llopis, and A. Maquieira, *Opt. Lett.* **35** (21), 3673 (2010).
5
6 [147] J. S. Foresi, P. R. Villeneuve, J. Ferrera, E. R. Thoen, G. Steinmeyer, S. Fan, J. D.
7 Joannopoulos, L. C. Kimerling, H. I. Smith, and E. P. Ippen, *Nature* **390** (6656), 143
8 (1997).
9
10 [148] S. Mandal and D. Erickson, *Opt. Express* **16** (3), 1623 (2008).
11
12 [149] S. Mandal, R. Akhmechet, L. Chen, S. Nugen, A. Baeumner, and D. Erickson, *Proced.*
13 *SPIE* **6645**, 6451J (2007).
14
15 [150] S. Mandal, J. M. Goddard, and D. Erickson, *Lab Chip* **9** (20), 2924 (2009).
16
17 [151] M. Lee and P. M. Fauchet, *Opt. Express* **15** (8), 4530 (2007).
18
19 [152] E. Guillermain and P. M. Fauchet, *Proc. SPIE* **7167**, 71670D (2009).
20
21 [153] S. Pal, E. Guillermain, R. Sriram, B. L. Miller, and P. M. Fauchet, *Biosens. Bioelectron.*
22 **26** (10), 4024 (2011).
23
24 [154] S. Zlatanovic, L. W. Mirkarimi, M. M. Sigalas, M. A. Bynum, E. Chow, K. M. Robotti,
25 G. W. Burr, S. Esener, and A. Grot, *Sens. Actuators B* **141** (1), 13 (2009).
26
27 [155] M. R. Lee and P. M. Fauchet, *Opt. Lett.* **32** (22), 3284 (2007).
28
29 [156] S. Mandal, X. Serey, and D. Erickson, *Nano. Lett.* **10** (1), 99 (2010).
30
31 [157] D. Erickson, X. Serey, Y.-F. Chen, and S. Mandal, *Lab Chip* **11** (6), 995 (2011).
32
33 [158] A. Densmore, D. X. Xu, P. Waldron, S. Janz, P. Cheben, J. Lapointe, A. Delage, B.
34 Lamontagne, J. H. Schmid, and E. Post, *IEEE Phot. Tech. Lett.* **18** (21-24), 2520
35 (2006).
36
37 [159] A. Densmore, D. X. Xu, S. Janz, P. Waldron, T. Mischki, G. Lopinski, A. Delage, J.
38 Lapointe, P. Cheben, B. Lamontagne, and J. H. Schmid, *Opt. Lett.* **33** (6), 596 (2008).
39
40 [160] D. X. Xu, M. Vachon, A. Densmore, R. Ma, S. Janz, A. Delage, J. Lapointe, P. Cheben,
41 J. H. Schmid, E. Post, S. Messaoudene, and J. M. Fedeli, *Opt. Express* **18** (22), 22867
42 (2010).
43
44 [161] A. Densmore, M. Vachon, D. X. Xu, S. Janz, R. Ma, Y. H. Li, G. Lopinski, A. Delage,
45 J. Lapointe, C. C. Luebbert, Q. Y. Liu, P. Cheben, and J. H. Schmid, *Opt. Lett.* **34** (23),
46 3598 (2009).
47
48 [162] D. X. Xu, M. Vachon, A. Densmore, R. Ma, A. Delage, S. Janz, J. Lapointe, Y. Li, G.
49 Lopinski, D. Zhang, Q. Y. Liu, P. Cheben, and J. H. Schmid, *Opt. Lett.* **35** (16), 2771
50 (2010).
51
52 [163] V. R. Almeida, Q. Xu, C. A. Barrios, and M. Lipson, *Opt. Lett.* **29** (11), 1209 (2004).
53
54 [164] F. Dell'Olio and V. M. N. Passaro, *Opt. Express* **15** (8), 4977 (2007).
55
56 [165] C. A. Barrios, *Sensors* **9** (6), 4751 (2009).
57
58 [166] C. A. Barrios, K. B. Gylfason, B. Sanchez, A. Griol, H. Sohlstrom, M. Holgado, and R.
59 Casquel, *Opt. Lett.* **32** (21), 3080 (2007).
60

- 1
2
3 [167] C. A. Barrios, M. J. Banuls, V. Gonzalez-Pedro, K. B. Gylfason, B. Sanchez, A. Griol,
4 A. Maquieira, H. Sohlstrom, M. Holgado, and R. Casquel, *Opt. Lett.* **33** (7), 708 (2008).
5
6 [168] C. F. Carlborg, K. B. Gylfason, A. Kazmierczak, F. Dortu, M. J. B. Polo, A. Maquieira
7 Catala, G. M. Kresbach, H. Sohlstrom, T. Moh, L. Vivien, J. Popplewell, G. Ronan, C.
8 A. Barrios, G. Stemme, and W. van der Wijngaart, *Lab Chip* **10** (3), 281 (2010).
9
10 [169] K. B. Gylfason, C. F. Carlborg, A. Kazmierczak, F. Dortu, H. Sohlstrom, L. Vivien, C.
11 A. Barrios, W. van der Wijngaart, and G. Stemme, *Opt. Express* **18** (4), 3226 (2010).
12
13 [170] A. D. Falco, L. O'Faolain, and T. F. Krauss, *Appl. Phys. Lett.* **92** (8), 083501 (2008).
14
15 [171] A. Di Falco, L. O'Faolain, and T. F. Krauss, *Appl. Phys. Lett.* **94** (6), 063503 (2009).
16
17 [172] M. Holgado, R. Casquel, B. Sanchez, C. Molpeceres, M. Morales, and J. L. Ocana, *Opt.*
18 *Express* **15** (20), 13318 (2007).
19
20 [173] D. Lopez-Romero, C. A. Barrios, M. Holgado, M. F. Laguna, and R. Casquel,
21 *Microelectron. Eng.* **87** (4), 663 (2010).
22
23 [174] M. Holgado, R. Casquel, C. Molpeceres, M. Morales, and J. L. Ocana, *Sensor Lett.* **6**
24 (4), 564 (2008).
25
26 [175] M. Holgado, C. A. Barrios, F. J. Ortega, F. J. Sanza, R. Casquel, M. F. Laguna, M. J.
27 Banuls, D. Lopez-Romero, R. Puchades, and A. Maquieira, *Biosens. Bioelectron.* **25**
28 (12), 2553 (2010).
29
30 [176] T. Braun, M. K. Ghatkesar, N. Backmann, W. Grange, P. Boulanger, L. Letellier, H.-P.
31 Lang, A. Bietsch, C. Gerber, and M. Hegner, *Nat. Nanotechnol.* **4** (3), 179 (2009).
32
33 [177] A. Salehi-Khojin, S. Bashash, N. Jalili, M. Muller, and R. Berger, *J. Appl. Phys.* **105**
34 (1), 013506 (2009).
35
36 [178] J. W. Ndieyira, M. Watari, A. D. Barrera, D. Zhou, M. Vogtli, M. Batchelor, M. A.
37 Cooper, T. Strunz, M. A. Horton, C. Abell, T. Rayment, G. Aeppli, and R. A.
38 McKendry, *Nat. Nanotechnol.* **3** (11), 691 (2008).
39
40 [179] M. Alvarez, A. Calle, J. Tamayo, L. M. Lechuga, A. Abad, and A. Montoya, *Biosens.*
41 *Bioelectron.* **18** (5-6), 649 (2003).
42
43 [180] M. Alvarez and L. M. Lechuga, *Analyst* **135** (5), 827 (2010).
44
45 [181] A. K. Naik, M. S. Hanay, W. K. Hiebert, X. L. Feng, and M. L. Roukes, *Nat.*
46 *Nanotechnol.* **4**, 445 (2009).
47
48 [182] N. Privorotskaya, Y.-S. Liu, J. Lee, H. Zeng, J. A. Carlisle, A. Radadia, L. Millet, R.
49 Bashir, and W. P. King, *Lab Chip* **10** (9), 1135 (2010).
50
51 [183] S. Singamaneni, M. C. LeMieux, H. P. Lang, C. Gerber, Y. Lam, S. Zauscher, P. G.
52 Datskos, N. V. Lavrik, H. Jiang, R. R. Naik, T. J. Bunning, and V. V. Tsukruk, *Adv.*
53 *Mater.* **20** (4), 653 (2008).
54
55 [184] S. W. Stahl, E. M. Puchner, and H. E. Gaub, *Rev. Sci. Instrum.* **80** (7), 073702 (2009).
56
57 [185] D. Rugar, R. Budakian, H. J. Mamin, and B. W. Chui, *Nature* **430** (6997), 329 (2004).
58
59
60

- 1
2
3 [186] K. Zinoviev, C. Dominguez, J. A. Plaza, V. c. J. C. Busto, and L. M. Lechuga, J.
4 Lightwave Technol. **24** (5), 2132 (2006).
5
6 [187] J. W. Noh, R. R. Anderson, S. Kim, W. Hu, and G. P. Nordin, Opt. Express **17** (22),
7 20012 (2009).
8
9 [188] J. W. Noh, R. R. Anderson, S. Kim, W. Hu, and G. P. Nordin, Nanotechnology **21** (15),
10 155501 (2010).
11
12 [189] R. Panergo, C.-S. Huang, C.-S. Liu, P. G. Reinhall, and W.-C. Wang, J. Lightwave
13 Technol. **25** (3), 850 (2007).
14
15 [190] T. Xu, M. Bachman, F.-G. Zeng, and G.-P. Li, Sens. Actuators A **114** (2-3), 176 (2004).
16
17 [191] S. T. Koev, R. Fernandes, W. E. Bentley, and R. Ghodssi, IEEE T. Biomed. Circ. S. **3**
18 (6), 415 (2009).
19
20 [192] M. Nordstrom, D. A. Zauner, A. Boisen, and J. Hubner, J. Lightwave Technol. **25** (5),
21 1284 (2007).
22
23 [193] A. Llobera, V. J. Cadarso, K. Zinoviev, C. Dominguez, S. Buttgenbach, J. Vila, J. A.
24 Plaza, and S. Biittgenbach, IEEE Photon. Technol. Lett. **21** (2), 79 (2009).
25
26 [194] M. W. Pruessner, N. Siwak, K. Amarnath, S. Kanakaraju, W.-H. Chuang, and R.
27 Ghodssi, J. Micromech. Microeng. **16** (4), 832 (2006).
28
29 [195] C. Lee, J. Thillaigovindan, C.-C. Chen, X. T. Chen, Y.-T. Chao, S. Tao, W. Xiang, A.
30 Yu, H. Feng, and G. Q. Lo, in *Appl. Phys. Lett.* (2008).
31
32 [196] W. H. P. Pernice, M. Li, and H. X. Tang, Opt. Express **17** (15), 12424 (2009).
33
34 [197] W. Xiang and C. Lee, IEEE J. Sel. Top. Quantum Electron. **15** (5), 1323 (2009).
35
36 [198] M. W. Pruessner, T. H. Stievater, M. S. Ferraro, W. S. Rabinovich, J. L. Stepnowski,
37 and R. A. McGill, Lab Chip **10** (6), 762 (2010).
38
39 [199] K. Zinoviev, C. Dominguez, and A. Vila, Opt. Express **13** (21), 8618 (2005).
40
41 [200] W. S. Hu, R. Anderson, Y. S. Qian, J. G. Song, J. W. Noh, S. Kim, and G. P. Nordin,
42 Rev. Sci. Instrum. **80** (8) (2009).
43
44 [201] K. Misiakos, I. Raptis, A. Gerardino, H. Contopanagos, and M. Kitsara, Lab Chip **9** (9),
45 1261 (2009).
46
47 [202] M. Li, P. H. P., and T. X., Nat. Photonics **3** (8), 464 (2009).
48
49 [203] M. Li, W. H. P. Pernice, C. Xiong, T. Baehr-Jones, M. Hochberg, and H. X. Tang,
50 Nature **456** (7221), 480 (2008).
51
52 [204] R. R. Anderson, W. Hu, J. W. Noh, W. C. Dahlquist, S. J. Ness, T. M. Gustafson, D. C.
53 Richards, S. Kim, B. A. Mazzeo, A. T. Woolley, and G. P. Nordin, Lab Chip **11** (12),
54 2088 (2011).
55
56 [205] M. D. LaHaye, O. Buu, B. Camarota, and K. C. Schwab, Science **304** (5667), 74
57 (2004).
58
59 [206] K. C. Schwab and M. L. Roukes, Phys. Today **58** (7), 36 (2005).
60

- 1
2
3 [207] J. D. Teufel, T. Donner, M. A. Castellanos-Beltran, J. W. Harlow, and K. W. Lehnert,
4 Nat. Nanotechnol. **4** (12), 820 (2009).
5
6 [208] J. D. Teufel, J. W. Harlow, C. A. Regal, and K. W. Lehnert, Phys. Rev. Lett. **101** (19),
7 197203 (2008).
8
9 [209] F. J. Blanco, M. Agirregabiria, J. Berganzo, K. Mayora, J. Elizalde, A. Calle, C.
10 Dominguez, and L. M. Lechuga, J. Micromech. Microeng. **16** (5), 1006 (2006).
11
12 [210] N. M. Jokerst, L. Luan, S. Palit, M. Royal, S. Dhar, M. A. Brooke, and T. Tyler, IEEE
13 T. Biomed. Circ. S. **3** (4), 202 (2009).
14
15 [211] K. B. Mogensen and J. P. Kutter, Electrophoresis **30** (S1), S92 (2009).
16
17 [212] J. J. Lillie, M. A. Thomas, N. M. Jokerst, S. E. Ralph, K. A. Dennis, and C. L.
18 Henderson, J. Opt. Soc. Am. B **23** (4), 642 (2006).
19
20 [213] in *PHYTIA European Union project* (www.pythia-project.eu).
21
22 [214] R. Osellame, H. J. W. M. Hoekstra, G. Cerullo, and M. Pollnau, Laser Photonic Rev. **5**
23 (3), 442 (2011).
24
25
26
27
28
29
30
31
32
33
34
35
36
37
38
39
40
41
42
43
44
45
46
47
48
49
50
51
52
53
54
55
56
57
58
59
60

Abstract Figure



For Peer Review

1
2
3 M^a Carmen Estevez graduated with a Bachelor of Chemistry in 1998. Subsequently she joined the
4 Spanish National Research Council (CSIC) where she started her research in the field of
5 immunochemistry and bioanalytical chemistry. She obtained her MSc and PhD in Chemistry from the
6 University of Barcelona in 1999 and 2005, respectively. After her PhD, she joined the University of
7 Florida in 2006 as Postdoctoral Researcher until 2008 where she focused on the production and
8 applications of fluorescent nanoparticles in bioanalytical applications. In 2009 she joined the
9 Nanobiosensors and Bioanalytical Applications group at the Research Center on Nanoscience and
10 Nanotechnology (CIN2) where she is focusing on surface biofunctionalization and clinical diagnostics
11 applications of label-free optical biosensors.



12
13
14
15
16
17
18
19
20
21
22
23
24 Mar Alvarez is a researcher at the Nanobiosensors and Bioanalytical Applications Group in the Research
25 Center on Nanoscience and Nanotechnology (CIN2) of the Spanish National Research Council (CSIC),
26 with a special interest in biotechnology and nanofabrication for biosensor devices. She is especially
27 involved in the development of nanomechanical-based biosensors and their integration in lab-on-chip
28 platforms for clinical diagnosis. She obtained her MSc and PhD degrees in Physics from the Autonomia
29 University of Madrid, Spain. After her PhD she joined Monash University (Melbourne, Australia) for a
30 post-doctoral experience.



31
32
33
34
35
36
37
38
39
40
41
42
43
44 Laura M. Lechuga is Full Professor of the Spanish National Research Council (CSIC). She is the Head of
45 the Nanobiosensors and Bioanalytical Applications Group at the Research Center on Nanoscience and
46 Nanotechnology (CIN2), CSIC. The principal focus of her research program is the development of
47 biosensor devices based on plasmonics, magnetoplasmonics, integrated photonics and nanomechanics
48 principles, including surface biofunctionalization, microfluidics and lab-on-a-chip integration. The
49 biosensing platforms are applied to the environmental control of pollutants, early diagnosis of cancer and
50 diseases and genomics and proteomics.



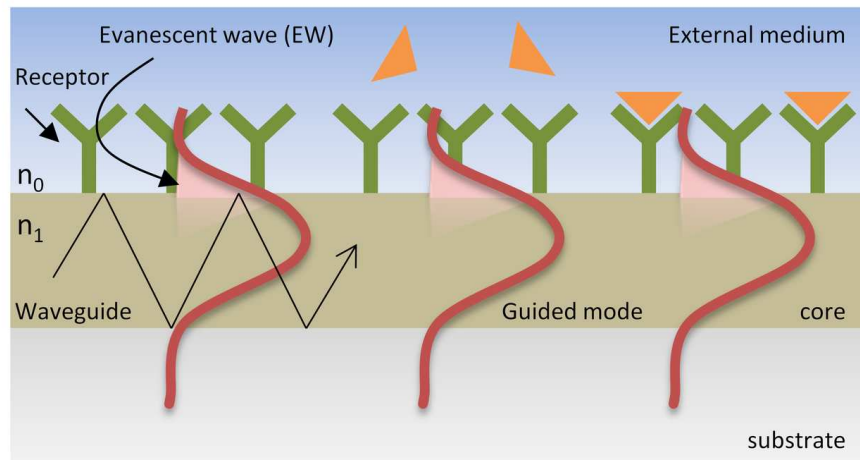


Figure 1. Scheme of the evanescent field sensing. A biomolecular interaction taking place at the waveguide surface within the evanescent region induces a change in the effective refractive index of the transmitted light mode. The evaluation of this optical change gives a measure of the number of molecules which has been detected.

59x32mm (600 x 600 DPI)

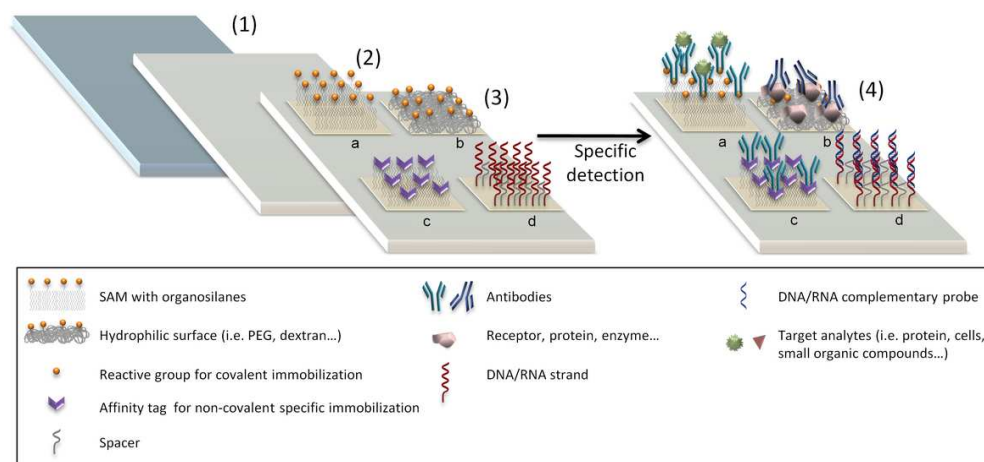


Figure 2. General scheme for the activation of the sensor surface and common strategies for biofunctionalization: surface cleaning (1), chemical activation of plain surface (2), immobilization of the specific bioreceptors (3) and final detection of the target molecule (4). The bioassays depicted in (3) and (4) are the following: (a) Mixed self-assembled monolayer (SAM) with reactive and non-reactive silanes compounds with specific antibodies covalently immobilized for protein recognition; (b) hydrophilic and biocompatible reactive monolayer based on pegylated-silane or dextran compounds with proteins covalently immobilized for antibody recognition; (c) Affinity tags immobilized on the surface (i.e. protein A, or streptavidin onto biotinylated surface) to achieve appropriate orientation of specific antibodies for protein recognition; (d) covalent immobilization of DNA or RNA probes (together with non-specific spacers) for hybridization with complementary DNA/RNA strands.

99x47mm (300 x 300 DPI)

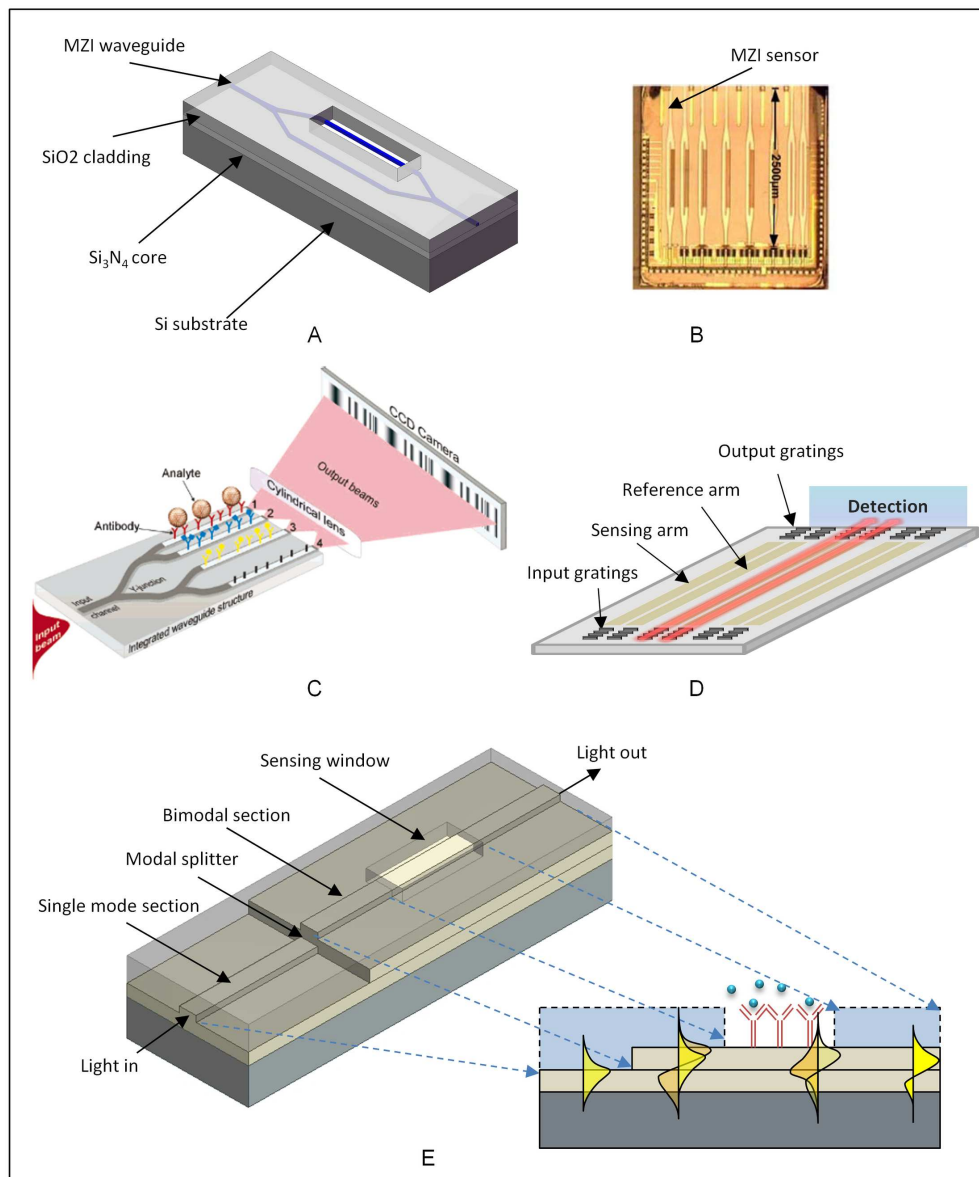


Figure 3. Several interferometric transducers for sensing: (A) Mach-Zehnder interferometer; (B) Mach-Zehnder interferometer sensor array with reference channels, reprinted from [210] with permission from IEEE (© 2009, IEEE); (C) Four Channel Young Interferometer, reprinted with permission from [56]. Copyright 2007 American Chemical Society; (D) Hartman Interferometer; (E) Bimodal Waveguide Interferometer.
189x225mm (300 x 300 DPI)

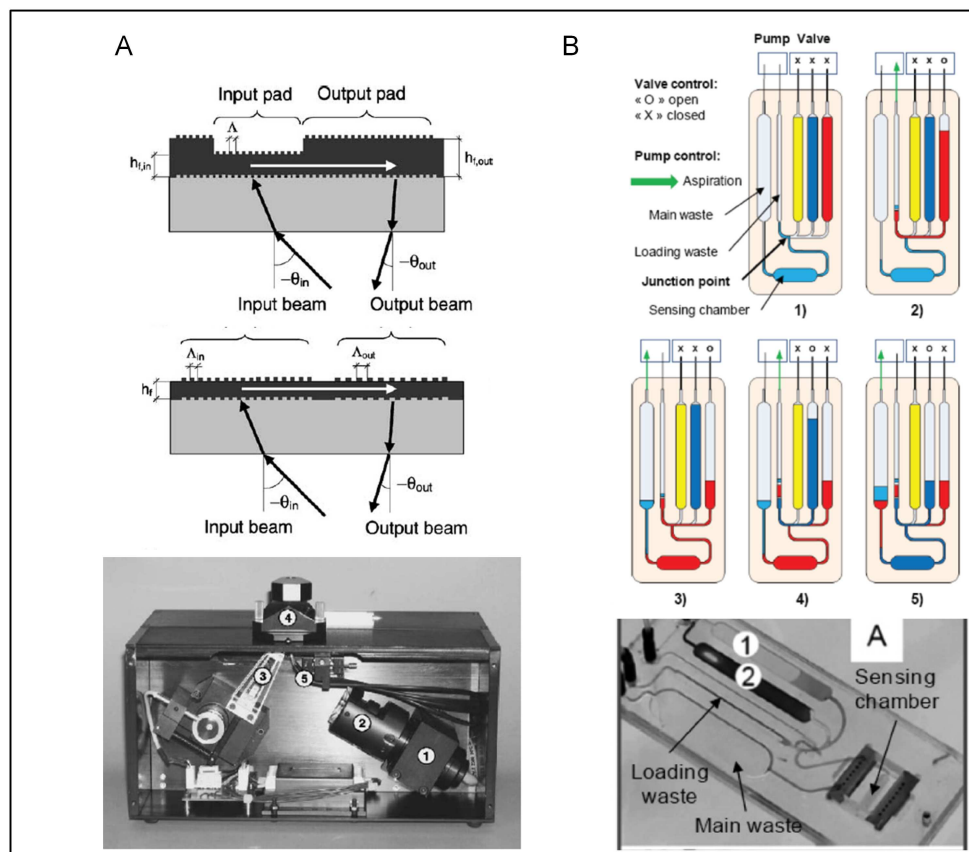


Figure 4. (A) Wavelength Interrogated Optical Sensor (WIOS) based on in and output grating couplers. Two different grating configurations are shown: a grating with different periods for in and output and a single grating with different thickness layer. Photograph of a compact WIOS instrument with (1) laser source, (2) beam expander, (3) deflection mirror, (4) sensing chip with fluidic cell, and (5) array of plastic optical fibers. Reprinted from [82] with permission from Elsevier.

(B) Lab-on-a-chip based on WIOS configuration adapted to a polymer-based self-contained microfluidic cartridge. Adapted and reproduced from [85] with permission of the Royal Society of Chemistry.

129x116mm (600 x 600 DPI)

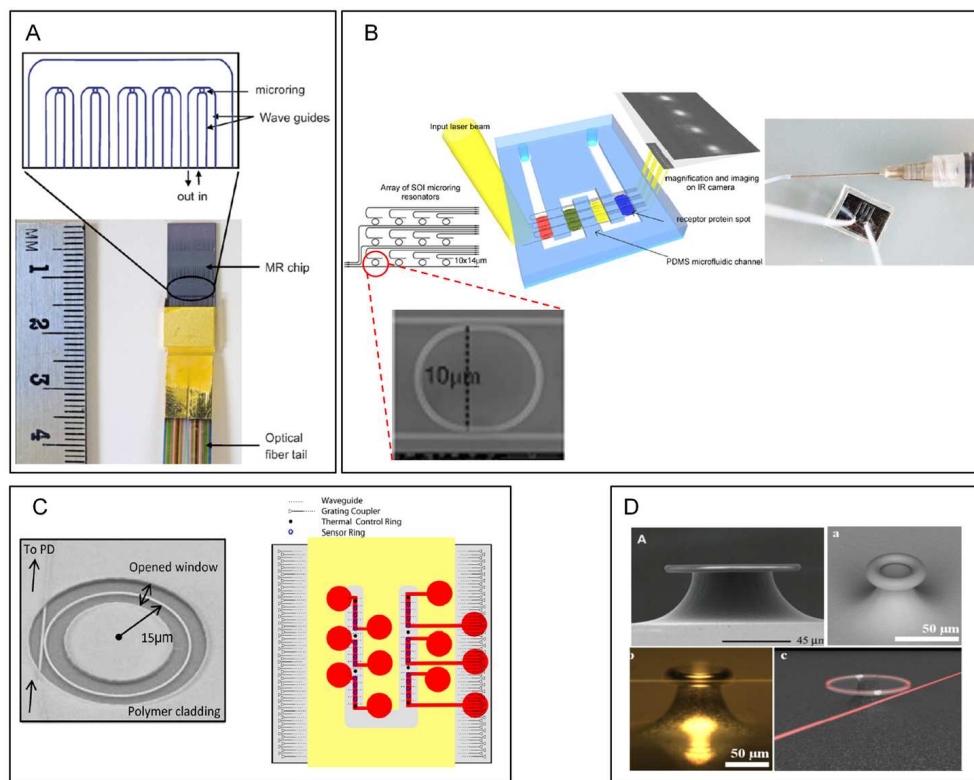


Figure 5. Several resonator sensing configurations: (A) Silicon chip with five rings vertically coupled to input and output port waveguides. Reprinted from [104] with permission from Elsevier. (B) Array platform of SOI-based ring resonators packaged with PDMS microfluidics. Reprinted from [112] with permission from IEEE (© 2009 IEEE) (C) SEM micrograph of a single ring with a window opened in the cladding polymer to expose the sensor surface. Microchip with 32 sensors and a six-channel PDMS microfluidic cell for multiplexed analyses. Reprinted from [96] and [116] with permission from IEEE (© 2010 IEEE) and from American Chemical Society, respectively. (D) Top: Scanning electron micrographs of microtoroids; Bottom: Microtoroids images showing the tapered fiber for incoupling of the light. Reprinted from [98] with permission from AAAS and from [101].
124x97mm (300 x 300 DPI)

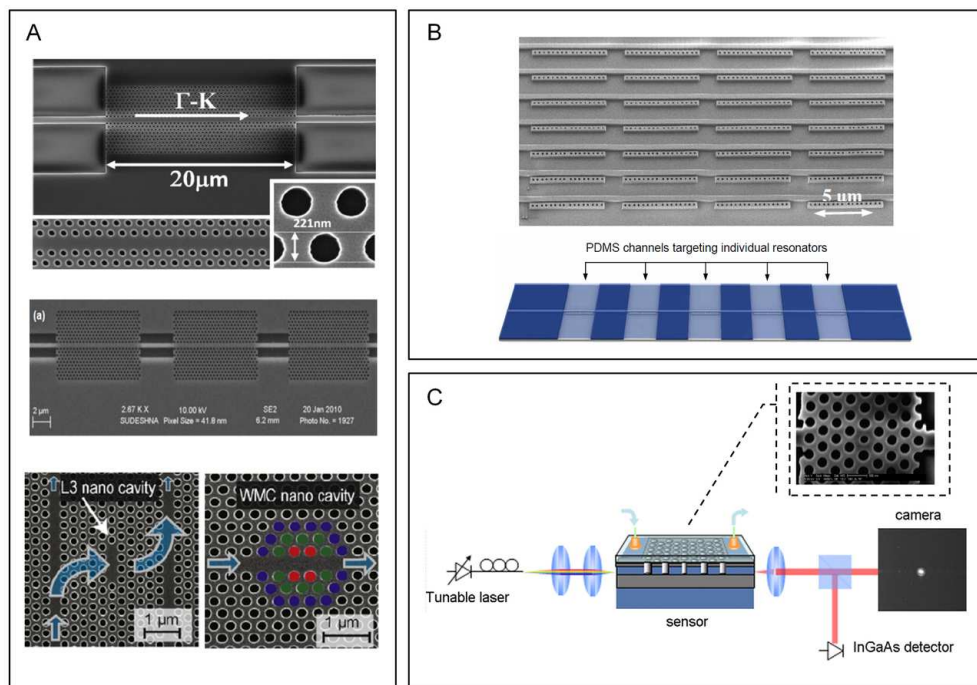


Figure 6. (A) SEM images of several photonic crystal-based waveguides sensors. Reprinted from [146] with permission from the Optical Society of America and from [143,153] with permission from Elsevier. (B) SEM image of a nanoscale optofluidic array of photonic crystal microcavities with multiplexed capabilities (top) and a scheme of a PDMS fluidic channel used for sample delivery (bottom). Reprinted from [148] with permission from the Optical Society of America. (C) Scheme of the evaluation set-up of a photonic crystal microcavity sensor, showing the optics (laser, fiber polarizer, input collimating and focusing optics, output objective, photodetector and alignment camera) and integrated microfluidics. SEM image of the photonic crystal structure is also included. Reprinted from [154] with permission from Elsevier.

109x78mm (300 x 300 DPI)

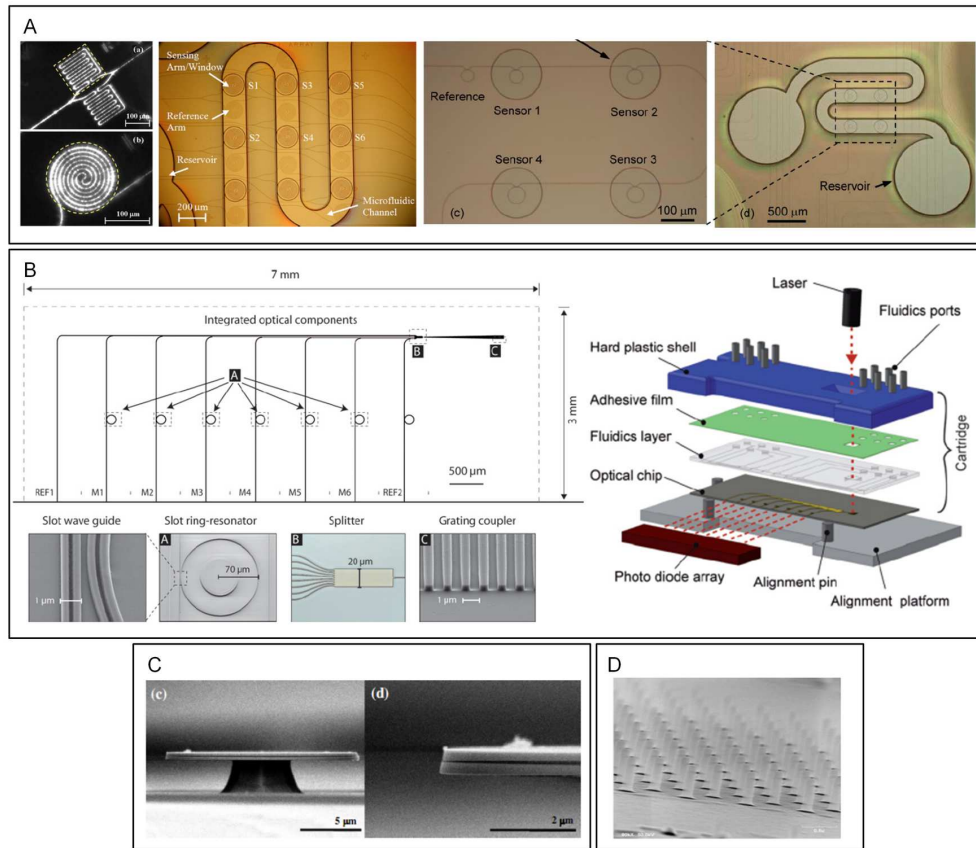


Figure 7. (A) Silicon photonic wire MZI and resonator sensor arrays. Details of the structures and the SU-8 microfluidic channels aligned to the sensor windows are shown. Reprinted from [159-161] with permission from the Optical Society of America. (B) Slot-waveguide ring resonator chip, consisting of 6 sensing channels plus 2 reference ones. Details of the structures and grating couplers of the resonator array (left) and the compact sensor cartridge for multiplexed sensing (right) are shown. Reprinted from [168] with permission of the Royal Society of Chemistry. (C) SEM images of fabricated air-slot disk with a diameter of 15 μm and an air slot depth of 2 μm. Reprinted from [89] with permission from the Optical Society of America. (D) SEM images of SU-8 nanocolumns lattices. Reprinted from [175] with permission from Elsevier.

149x128mm (300 x 300 DPI)

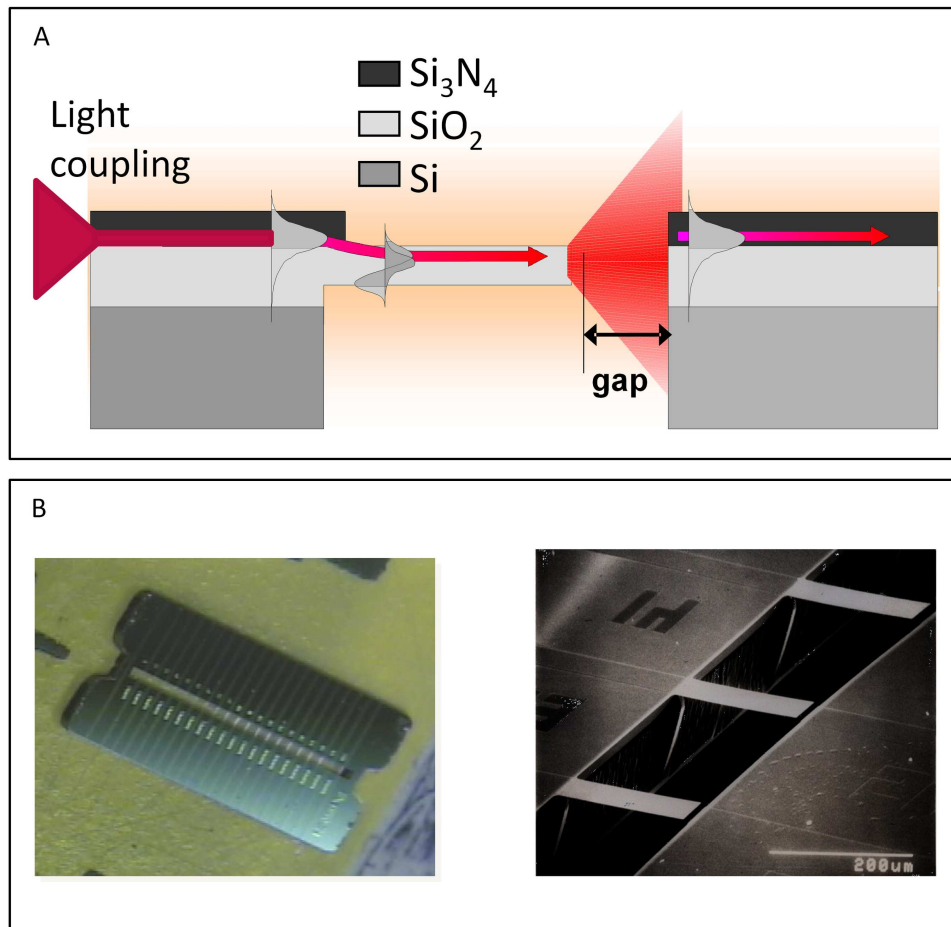


Figure 8. (A) Schematic representation of the optical waveguide cantilever (OWC) working principle. Input light is coupled to the cantilever through the evanescent field of an input waveguide, and output light is collected in a misaligned waveguide after crossing a small gap. (B) Picture and SEM image of an OWC chip array with 20 waveguide microcantilevers. Reproduced from [180] with permission of the Royal Society of Chemistry.
119x119mm (600 x 600 DPI)

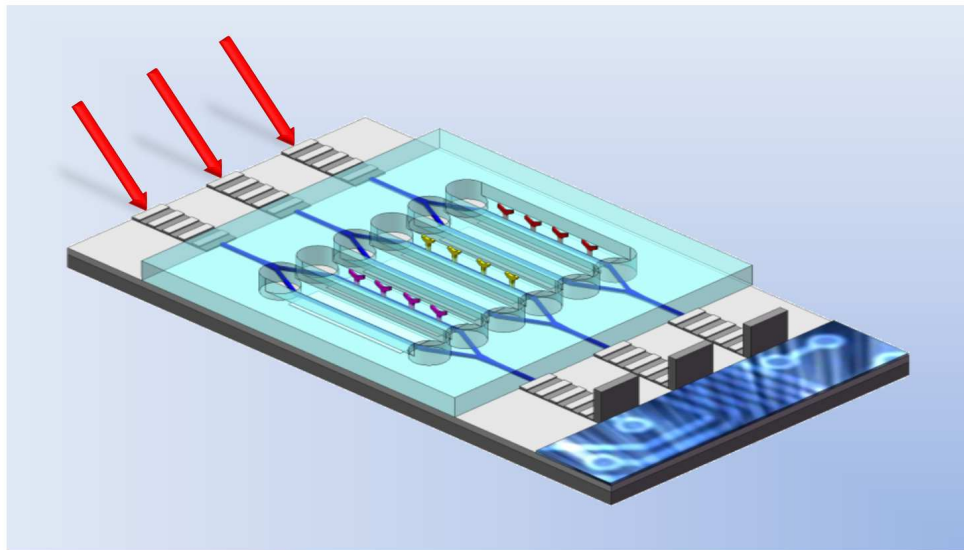


Figure 9. Envisioned lab-on-a-chip platform with on-chip detection using integrated optics-based transducers. In the figure, an array of Mach-Zehnder interferometers are integrated with individual microfluidics channels, grating couplers for the in and output of the light in each sensing channel, read-out photodetectors and CMOS electronics for data processing.
63x35mm (600 x 600 DPI)

Table 1. Comparison of limit of detection (LOD) in integrated optical biosensors

Device	Mass detection limit (pg/mm ²)	RI detection limit (RIU)	References
SPR ^a	1-5 ^(a,b)	10 ⁻⁵ -10 ⁻⁷	[4]
Grating Couplers			
Input and/or/output	n.d. ^(c)	~2·5·10 ⁻⁶	[64,66]
	0.3	<10 ⁻⁶	[82]
Reflected mode	10	3·10 ⁻⁶	[73;74]
Interferometer			
Mach Zehnder	n.d.	7·10 ⁻⁶	[41]
	0.06	1·10 ⁻⁷	[44]
	0.01 ^(d)	2·10 ^{-8(d)}	[12]
	n.d.	9.2·10 ⁻⁷	[212]
	n.d.	5·10 ⁻⁶	[52]
Young	0.75	9·10 ⁻⁸	[47]
	0.013 ^(d)	9·10 ⁻⁹	[48]
	0.020 ^(d)	8.5·10 ⁻⁸	[54]
Hartman	n.d.	~10 ⁻⁶	[60]
Bimodal waveguide	n.d.	2.5·10 ⁻⁷	[61]
Microring resonator			
	n.d.	~10 ⁻⁵	[92]
	3.4 ^(d)	n.d.	[112]
	15 / 1.5 ^(d)	7.6·10 ⁻⁷	[96,97]
Photonic Crystals			
	0.42	3.4·10 ⁻⁵	[124]
	500	~10 ⁻³	[142,143]
	2.1 ^(d)	6·10 ⁻⁴	[145]
	7.5 ^(d)	7·10 ⁻⁵	[148,150]
	1000	n.d.	[153]
Silicon Wires			
Mach-Zehnder configuration	0.25 ^(d)	n.d.	[161]
Resonator configuration	n.d.	<2·10 ⁻⁶	[162]
Slot-waveguides			
	16	n.d.	[167]
	n.d.	8.8·10 ⁻⁶	[169]
	0.9	5·10 ⁻⁶	[168]
	n.d.	4.2·10 ⁻⁵	[95]
	n.d.	7·10 ⁻⁶	[171]

^a: SPR is shown for comparison of the platforms with a standard optical biosensing device

^b: averaged

^c: n.d. not determined

^d: estimated

Table 2. Current commercial technologies based on integrated optics biosensing^(a)

Company	Instrument	Technology	Format	Throughput	Webpage
Farfield	AnaLight	Young Interferometry	Flow conditions	Low	www.farfield-group.com
SRU Biosensing	BIND Biosensor	Photonic Crystal	Cartridge (16) Microplate (96-1536)	Very High	www.srubiosystems.com
Corning	EPIC System	Waveguide Resonant Grating	Microplate (384)	High	www.corning.com
Axela	DotLab	Optical Grating	Flow/static conditions	Medium	www.axelabiosensors.com
Microvacuum	OWLS	Optical Grating Couplers	Flow conditions	Low	www.owls-sensors.com
Genalyte	Maverick	Ring resonators	Consumable with 1 to 128 resonators	Medium	www.genalyte.com

^a: Sensitivity levels are in the low ng/mL range in all the cases.

For Peer Review